Comparison of immunogenicity and protection efficacy of self-amplifying and circular mRNA vaccines against SARS-CoV-2

Oinam Ningthemmani Singh[1], Umang Berry[1], Garima Joshi[2], Tejeswara Rao Asuru[2], Kannan Chandrasekar[1], Sriram Narayanan[3], Puneet Srivastava[1], Mahima Tiwari[1], Souvick Chattopadhyay[4], Farha Mehdi[4], Bhisma Narayan Panda[5], Debasis Nayak[6], Shailendra Mani[1], Tripti Shrivastava[1], Gaurav Batra[4], C.T. Ranjith-Kumar[3], Prasenjit Guchhait[2], Milan Surjit[1*]

[1]Centre for Virus research, therapeutics and vaccines, Translational Health Science and Technology Institute, National Capital Region Biotech Science Cluster, Faridabad, Haryana, India.

[2]Regional Centre for Biotechnology, National Capital Region Biotech Science Cluster, Faridabad, Haryana, India.

[3]University School of Biotechnology, Guru Gobind Singh Indraprastha University, New Delhi, India.

[4]Centre for Biodesign, Translational Health Science and Technology Institute, National Capital Region Biotech Science Cluster, Faridabad, Haryana, India.

[5]Experimental animal facility, Translational Health Science and Technology Institute, National Capital Region Biotech Science Cluster, Faridabad, Haryana, India.

[6]Department of Biological Science, Indian Institute of Science Education and Research (IISER) Bhopal IISER, Bhopal, India.

Correspondence: milan@thsti.res.in

Abstract

Recent advances in vaccine technology have positioned messenger RNA (mRNA) vaccines as safe and reliable options for human use. Conventionally, mRNA vaccines were designed using linear or self-amplifying mRNA (SAM), the latter considered to be superior. However, limited success was achieved with SAM vaccines during the COVID-19 pandemic. Further, studies on Circular mRNA (Circ-RNA) vaccines against the SARS-CoV-2, Ebola and monkey pox proved their efficacy. Circ-RNAs are highly stable, neither they induce inflammatory response nor require any extracellular protein for their function. Here, we compared the efficacy of SAM- and Circ-RNA vaccines using the SARS-CoV-2-RBD (receptor binding domain) as the antigen. Both SAM-RBD and Circ-RBD induced a comparable anti-RBD IgG titer and virus-neutralizing antibody titer. However, the latter induced a significantly higher memory T-cell response. Immunization with SAM- and Circ-RBD showed no mortality and improved lung pathophysiology against acute SARS-CoV-2 infection in mice. The Circ-RBD vaccine is stable for 4 weeks at 4^0C. A bivalent vaccine containing Circ-RBD of both delta and omicron SARS-CoV-2 variants potently neutralized these viruses. These findings demonstrate Circ-RNA-RBD as an excellent vaccine candidate against COVID-19 and also provide a platform for developing bivalent Circ-RNA vaccine candidates against SARS-CoV-2 or other viruses with rapidly emerging variants.

Introduction

Although messenger RNA (mRNA) vaccines have been researched for more than two decades, its proof of success in real-life was witnessed for the first time during the COVID-19 pandemic. Comirnaty, the first FDA (United States food and drug administration)-approved COVID-19 vaccine (developed by Pfizer-BioNTech) and Spikevax (COVID-19 vaccine developed by Moderna), both mRNA vaccines, were pivotal in controlling the COVID-19. Since then, there is considerable momentum to develop mRNA vaccines against multiple pathogens, allergic diseases and cancer (Thomas et al., 2021; Baden et al., 2021; Arevalo et al., 2022; Krienke et al., 2021; Heine et al., 2021; Parhiz et al., 2024). Advances in mRNA delivery technology, *in vitro* transcription technology and reduction in the cost of production have improved the overall yield, stability, efficacy and economic viability of the mRNA vaccine, thereby positioning it as the preferred option for vaccine development (Chaudhary et al., 2021). Both linear mRNA (such as Comirnaty and Spikevax) and self-amplifying mRNA (SAM) (such as Gemcovac)-based vaccines have been approved for use in human (Thomas et al., 2021; Baden et al., 2021; Saraf et al., 2024). More recently, several independent studies have demonstrated the efficacy of circular mRNA (Circ-RNA) vaccines (Qu et al., 2022; Amaya et al., 2023; Seephetdee et al., 2022; Zhou et al., 2024).

Linear mRNA-encoding the vaccine antigen is generally small in size (compared to the SAM), contain a methyl-guanosine cap analog at the 5'-end, poly A-tailed at the 3'-end and the antigen-encoding sequence is flanked by untranslated regions (UTR) at both sides. A major challenge of linear mRNA-based vaccines is low stability of the input mRNA. Stability of the linear mRNAs are increased by incorporating pseudo-uridine or N6-Methyladenosine (m6A) into the sequence (Karikó et al., 2008; Wang et al. 2014). SAM vaccines are generally based on engineered genome of alphaviruses such as the Venezuela Equine Encephalitis virus (VEEV), Semliki Forest Virus (SFV) or Sindbis virus (SINV) (Bloom et al., 2020). Here, the viral structural protein-encoding sequence is replaced with the sequence of the vaccine antigen so that non-structural proteins of the virus enables replication the viral genome without production of infectious progeny virions. Thus, SAM vaccines should produce the required quantity of antigen for a prolonged period with less amount of the input RNA (compared to the linear mRNA), leading to a stronger and more durable immune response (Schmidt and Schnierle, 2023). However, use of viral replication machinery for amplifying the input RNA has certain disadvantages such as: size of the SAM RNA is considerably longer as it contains the sequence to express viral non-structural proteins; viral RNA-dependent RNA polymerase, which is required for replication of the SAM RNA has low fidelity, increasing the possibility of introducing mutation(s) in the antigen-encoding sequence; pre-existing anti-vector immunity remains a concern; generation of dsRNA during the replication of SAM might activate host defence machinery leading to degradation of SAM; possibility of uncontrolled and excessive replication of SAM due to mutations in the non-structural proteins cannot be ruled out. Notably, one of the SAM vaccines (COVAC1) failed to induce 100% seroconversion while another SAM

vaccine (ARCT154) showed a very good response in phase I clinical trials (Pollock et al., 2022; Oda et al., 2024). Gemcovac (Gennova), a commercially available SAM vaccine, also shows very good protection efficacy in clinical trials (Saraf et al., 2024).

Circular RNAs (Circ-RNA) are covalently closed single-stranded RNA without free 5'- and 3'-ends. It is produced naturally through back-splicing, which involves the connection of the 3'-end of an exon to the 5'- end of another exon, creating a close loop RNA. The circular structure provides resistance to most of the RNases except RNase A, RNase T1 and RNase T2, thus significantly increasing their half-life compared to linear mRNAs. Endogenous Circ-RNAs act as miRNA sponges to regulate various cellular processes by binding to nucleic acids and proteins, thereby modulating transcription and cellular signalling pathways (Liu and Chen, 2022). Circ-RNAs do not induce the cellular innate immune pathway RNA sensors (Wesselhoeft et al., 2019; Breuer et al., 2022). Recent reports have demonstrated the ability of engineered Circ-RNAs to express the vaccine antigens using internal ribosomal entry site (IRES)-mediated translation, thereby eliminating the requirement of capping of the 5'-end of the mRNA (Wesselhoeft et al., 2018a; Qu et al., 2022). Circ-RNA-based vaccines against the Severe acute respiratory syndrome-coronavirus-2 (SARS-CoV-2) and Monkey pox has been shown to induce potent immune response and protect the animals from challenge with the respective viruses (Qu et al., 2022; Zhou et al., 2024). Notably, in the case of SARS-CoV-2, Circ-RNA immunization produced a higher T_H1 biased humoral immune response and a higher neutralizing to binding antibody ratio than its mRNA counterpart, supporting its protection efficacy and superior potential for evading the antibody-dependent enhancement (ADE) (Qu et al., 2022).

SARS-CoV-2, the causative agent of the coronavirus-induced disease-19 (COVID-19), is responsible for the worst global pandemic of the 21st century. So far approximately 776 million COVID-19 cases and 7 million deaths have been reported globally (https://data.who.int/dashboards/covid19). The viral genome shows high mutation rate, leading to emergence of multiple variants, some of which, such as the B.1.617.2 (Delta) and the Omicron B.1.1.529 (BA.1) variants pose serious health issues (Tao et al., 2021; Carabelli et al., 2023). Omicron B.1.1.529 (BA.1) became the most dominant circulating strain with 22 subvariants accounting for 87% of infections. Omicron strain dominated the previous variant of concern (VOC) in 2022 and carries the most significant number of mutations than the previous VOC, with 37 mutations within its spike protein. 15 mutations at the RBD region covering almost all the critical mutation sites, such as K417N, S477N, T478K, E484A and N501Y make more transmissible and immune evasion to pre-existing immunity. Previous non-Omicron infection or vaccination has little protection against the Omicron variant (Cameroni et al., 2021; Liu et al., 2022; Planas et al., 2022). The Omicron sub-variants, including the BA.4/5 and XBB, continue to emerge, with total immune escaping potential to the previous vaccination. Few studies have shown the broader protective efficacy of bivalent mRNA and nanoparticle vaccines composed of a mixture of antigens from the SARS-CoV-2-Beta and Delta or Delta and Omicron variants (Yuan et al., 2022; Corleis et al., 2023; Schmidt and

156 Schnierle, 2023). Despite development of several vaccines against the SARS-CoV-2, there is
157 limited access to vaccines globally and there is scope for improving the efficacy and duration
158 of protection offered by the vaccines.
159 Being the viral outer surface protein, spike protein of the SARS-CoV-2 is the main target for
160 vaccine development. The receptor binding domain (RBD) of the spike protein, which accounts
161 for one-fifth of the total protein, produced over 90% of the neutralizing antibody in infected
162 patients (Piccoli et al., 2020). There are no reports of antibody dependent enhancement (ADE)
163 by vaccines based on the full length spike protein of the SARS-CoV-2. However, possibility of
164 ADE induction by the spike protein of emerging SARS-CoV-2 variants cannot be ruled out.
165 Therefore, RBD would be the best target for developing SARS-CoV-2 vaccines.
166 In the present study, we compared the immunogenicity and virus neutralization potential of
167 the Circ-RNA and SAM-RNA vaccine candidates using the SARS-CoV-2-RBD as the vaccine
168 antigen. Although both Circ-RBD (Circ-RNA backbone) and SAM-RBD (SAM-RNA backbone)
169 elicited comparable humoral and neutralizing antibody response, the former induced a
170 significantly higher T_H1-biased cellular immune response and protected mice from challenge
171 with the SARS-CoV-2. Further, Circ-RBD vaccine was stable in refrigerator, induced a durable
172 neutralizing antibody response and a bivalent vaccine formulation encoding the RBD of Delta
173 (Circ-RBD^{Del}) and Omicron (Circ-RBD^{Omi}) variants induced high cross-neutralizing antibody
174 response against both variants, confirming the protective efficacy of the Circ-RNA vaccines.
175 Significance of these findings in designing better mRNA vaccines based on circular RNA
176 technology is discussed.
177

178 **Results**

179 **Production and characterization of the SARS-CoV-2 SAM-RBD and Circ-RBD**
180 **vaccine formulations**

181 Self-splicing property of the Anabaena intron (Group 1) was utilized to generate the Circ-RNA
182 encoding the SARS-CoV-2-RBD (Wuhan isolate) fused to the CD5 signal sequence (SS) and
183 the sequence encoding the trimerization motif of bacteriophage T4 fibritin (foldon) at the N-
184 and C- terminus, respectively. The fusion protein was translated under control of a Coxsackie
185 virus B3 (CVB3) internal ribosome entry site, as reported earlier (Wesselhoeft et al., 2018a).
186 A bacteriophage T7 promoter sequence was placed upstream of the anabaena intron
187 sequence at the 5'-end to enable *in-vitro* transcription-mediated synthesis of Circ-RBD. A
188 Semliki Forest virus (SFV) replicon was engineered to produce the self-amplifying RNA
189 encoding the SARS-CoV-2-RBD (SAM-RBD). RBD-encoding sequence fused to the CD5
190 signal sequence and T4 fibritin foldon sequence at its 5'- and 3'-ends was inserted into the
191 SFV replicon. *In-vitro* transcription was carried out using the SP6 polymerase, followed by
192 Cap1-capping of the RNA. Sized integrity of the RNAs were verified by spectrophotometry and
193 formaldehyde-agarose gel electrophoresis. Expected sized of the RNAs were observed
194 (Figure 1A). An aliquot of the RNAs were treated with the RNase R to check their

circularization status. SAM-RBD was completely digested by RNase R treatment whereas majority of Circ-RBD was resistant, confirming its circularization (Figure1A). Next, RNA was encapsulated into the lipid-nanoparticle (LNP) by microfluidic mixing and the diameter of the resulting RNA-LNP formulation was measured. The average diameter of the SAM-RBD-LNP and the Circ-RBD-LNP was found to be 140 and 136nm, respectively (Figure 1B). Average polydispersity index (PDI) of the SAM-RBD-LNP and the Circ-RBD-LNP was 0.06 and 0.04, respectively (Figure 1C). LNP encapsulation and stability of the SAM-RBD and the Circ-RBD RNA in the LNP complex was verified by resolving the RNA-LNP complex with or without treatment with Triton X-100 (disrupts the LNP). No RNA was visible in the SAM-RBD-LNP and the Circ-RBD-LNP complex-containing samples (Figure 1D). Treatment of the sample with Triton X-100 results in detection of the SAM-RBD and Circ-RBD (Figure 1D). No difference was observed in the quality of the SAM-RBD and Circ-RBD RNA before and after LNP encapsulation (Figure 1D). Percentage LNP encapsulation of the SAM-RBD and Circ-RBD RNA was quantified using Ribogreen. 98.3% and 95.9% of SAM-RBD and Circ-RBD RNA, respectively, was LNP-encapsulated (Figure 1E). Scanning electron microscopy analysis of the SAM-RBD-LNP and Circ-RBD-LNP complexes revealed spherical structure with average diameter of 136nm and 149nm respectively (Figure 1F). Next, SAM-RBD-LNP and Circ-RBD-LNP complexes were transfected into HEK293T cells to detect the expression of RBD. Western Blot analysis of the whole cell extract using the anti-RBD antibody confirmed expression of the RBD protein (Figure 1G, upper panel). An aliquot of the whole cell extract was probed using the anti-GAPDH antibody to check equal loading of the sample (Figure 1G, lower panel). Secretion of RBD protein into the culture medium was checked by anti-RBD western blot of the culture medium collected from the cells used in the above experiment (shown in Figure 1G). RBD was detected in the culture medium as 2 distinct bands, likely representing the glycosylated variants of the same protein (Figure 1H). Aliquots of the same sample were resolved in non-reduced state to check trimerization status of the RBD protein. As expected, anti-RBD western blot detected a band of approximately 100kDa in the non-reduced samples, indicative of RBD-trimer (Figure 1I). Possible activation of the innate immune pathways by the SAM-RBD and Circ-RBD RNAs were checked by RT-qPCR analysis of IFN-β, RIG-I, OASL, PKR and OAS1 genes. None of these genes were induced by either of the RNAs (Figure 1J). As a positive control, cells were transfected with poly I:C in parallel, which is known to induce the cellular antiviral response pathway (Figure 1J). Collectively, these results confirmed LNP encapsulation of SAM-RBD and Circ-RBD RNA and expression of RBD protein trimer by both the RNAs. Importantly, western blot analysis also demonstrated that approximately same amount of RBD was produced by both the SAM-RBD and the Circ-RBD. Therefore, our experimental condition was suitable to compare the immune response induced by the SAM-RBD and the Circ-RBD.

233 **SAM-RBD and Circ-RBD RNA vaccines induced significant T_H1-biased humoral and**
234 **cellular immune response in mice**
235 To select the injection route and the optimal RNA dose, Balb/c mice were immunized via
236 intradermal (ID) or intramuscular (IM) route with freshly prepared vaccine formulation
237 containing 25μg Circ-RBD RNA. Two weeks later, immunization was repeated and blood was
238 collected after four weeks (day 28). Both ID and IM routes showed similar anti-RBD IgG titer
239 (average values: $6X10^5$ and $1X10^6$, respectively) and virus neutralization titer (average NT_{50}=
240 $1.7X10^3$ and $1.9X10^3$, respectively) (Figures S1A and B). ID immunization route was selected
241 for all subsequent experiments. Next, mice were injected with 5, 10 and 25μg of Circ-RBD-
242 RNA containing vaccine formulations in a two-dose immunization schedule as described
243 above. Measurement of anti-RBD IgG titer revealed average values to be $2.2X10^4$, $2.8X10^5$,
244 $6X10^5$ and average virus neutralization titer (NT_{50}) was found to be $0.5X10^3$, $1.5X10^3$, $0.8 X10^3$,
245 in 5, 10 and 20μg RNA containing formulations, respectively (Figures S1C and S1D). There
246 was no significant difference in values obtained between all 3 doses, hence 10μg RNA
247 containing formulation was selected for all subsequent experiments.
248 In order to evaluate the immune response generated by the Circ-RBD and SAM-RBD, 10μg
249 of each RNA containing vaccine formulation was intradermally injected into Balb/c mice in two
250 dose immunization schedules at two-week interval, followed by collection of blood and spleen
251 samples for analysis of different immune parameters (Figure 2A). Significant level of anti-RBD
252 IgM was detected in the sera of mice immunized with both SAM-RBD and Circ-RBD RNA
253 (Figure 2B). Importantly, no significant difference was observed in the level of IgM between
254 SAM-RBD and Circ-RBD immunized mice (Figure 2B). Measurement of anti-RBD IgG titer
255 and virus neutralization titer (NT_{50}) in the sera collected on day 28 from SAM-RBD and Circ-
256 RBD immunized mice revealed the average values to be $2.8X10^5$ and $3.2X10^5$ (anti-RBD-IgG
257 titer) and $1X10^3$ and $1.5X10^3$ (NT_{50}), respectively (Figures 2C and 2D). IgG-isotyping of
258 aliquots of the same sera showed comparable values between SAM-RBD and Circ-RBD
259 groups (Figures 2E-2G). The ratio of anti-RBD (IgG2a+IgG2b) to IgG1 was found to be 1.9
260 and 1.8, respectively, indicating a T_H1 response (Figure 2H). Next, splenocytes from these
261 mice were cultured *in vitro* and induced with overlapping peptide pool corresponding to the
262 RBD region, followed by selection of $CD4^+$ and $CD8^+$ T cells and quantification of intracellular
263 T_H1 (IFN-γ, TNF-α) and T_H2 (IL-4) cytokines. Both $CD4^+$ and $CD8^+$ T cells of mice immunized
264 with Circ-RBD induced significant IFN-γ and TNF-α response (Figures 2I-2L). A significant
265 IFN-γ and TNF-α response was observed in $CD4^+$ and $CD8^+$ T cells, respectively, in SAM-
266 RBD immunized mice (Figures 2I and 2L). An increased trend was observed in IFN-γ and
267 TNF-α level in $CD8^+$ and $CD4^+$ T cells, respectively, in SAM-RBD immunized mice although it
268 was not statistically significant (Figures 2J and 2K). There were no significant changes in IL-4
269 response in both SAM-RBD and Circ-RBD immunized mice, indicating that both vaccine
270 formulations induced T_H1-biased T-cell immune response (Figures 2M and 2N).
271 Representative FACS plots are shown (Figure S2). Collectively, these results demonstrate

272 that both SAM-RBD and Circ-RBD induced a robust and comparable humoral immune
273 response, however, the latter induced a better T_H1-biased cell-mediated immune response.
274
275 **Immunization with the SAM-RBD and Circ-RBD RNA vaccines protect mice from the**
276 **SARS-CoV-2 infection and prevents COVID-19 associated pathological changes**
277 In order to evaluate the protection efficacy of the Circ-RBD vaccine, we established a mouse
278 model of the SARS-CoV-2 infection that produces a severe disease phenotype. Intratracheal
279 administration of the replication deficient adenovirus expressing the human angiotensin
280 converting enzyme 2 (Ad5CMV-hACE2, denoted as hACE2 hereafter) has been shown to
281 express the hACE2 in mouse lungs within 5 days of transduction (Gu et al., 2021). We
282 hypothesized that increased hACE2 expression in the lungs will permit more pronounced
283 SARS-CoV-2 infection in the lungs, leading to a more severe disease phenotype. To test the
284 hypothesis, mice were transduced with the hACE2 via intratracheal administration, followed
285 by intranasal infection with the 10^5 PFU of SARS-CoV-2 (Wuhan isolate), as described
286 (Hassan et al., 2020). Body weight of the animals were measured every day, blood was
287 collected prior to infection and upto 3 weeks after infection. Survivability of the animals were
288 monitored. Few animals were sacrificed each week and blood and lung tissue were collected
289 for analysis. Results obtained in the pilot experiment confirmed that our animal model
290 displayed a more severe pathogenic effect, including lethality in some animals. Protection
291 efficacy of the SAM-RBD and Circ-RBD RNA vaccines were compared in the above model.
292 Mice were immunized twice at 2 weeks intervals, followed by intratracheal transduction of the
293 hACE2 (on day 28). 10^5 PFU of the SARS-CoV-2 (Wuhan) was intranasally administered after
294 5 days and disease parameters were followed up for next three weeks (up to day 54). The
295 experimental plan is summarized (Figure 3A). In the placebo group, there was a marked
296 reduction in the body weight from the 2nd day of infection up to the 7th day, after which there
297 was a gradual increase in the body weight up to the 21st day (Figure 3B). In the case of SAM-
298 RBD and Circ-RBD vaccine immunized group, weight loss was observed between the 2nd to
299 4th day post-infection after which the animals gained weight, indicating that both vaccines
300 protected the animals from progressing to severe disease pathology (Figure 3B). Placebo
301 group animals appeared sick, displayed hunchback posture, barely moved and importantly,
302 three animals died during the observation period (one animal each died on day 36, 38 and 40)
303 (Figure 3C). The remaining animals started to gain weight from day 41 onwards. Notably,
304 SAM-RBD and Circ-RBD vaccine immunized animals were almost normal throughout the
305 observation period.
306 Anti-RBD IgG titer was measured in the placebo and vaccinated groups on day 33, 40, 47 and
307 54. There was no anti-RBD IgG in the placebo group on day 33 and an average titer of $5*10^3$
308 was observed after one week of infection, which increased upto 10^5 by day 54 (Figure 3D).
309 SAM-RBD vaccine immunized group showed an average anti-RBD IgG titer of 10^5-10^6 in the
310 samples collected between 33-54 days whereas Circ-RBD vaccine immunized group showed
311 an average anti-RBD IgG titer of 10^6 (Figure 3D). Estimation of viral RNA level and viral load

312 in the lung revealed higher viral RNA level (approximately ten-fold higher) and higher viral load
313 (10^3 PFU/mg of lung) in the lung tissue of placebo group (samples collected on day 40)
314 compared to the SAM-RBD and Circ-RBD vaccine immunized groups (Figures 3E, S3A). Both
315 viral RNA level and viral load were significantly less in the placebo group samples collected
316 on day 47 and 54, which inversely correlated with the anti-RBD IgG titer observed at the same
317 time point (Figures 3E, S3A). Morphology and histopathology analysis of lung tissue of
318 placebo group collected on day 40 showed multiple lesions, pneumonia and infiltration of
319 inflammatory cells whereas SAM-RBD and Circ-RBD vaccine immunized lung samples were
320 significantly better (Figures 3F, 3G). A similar profile was observed in the lung samples
321 collected on day 47 and 54 (Figures S3B, S3C). Quantification of lung infiltration score in the
322 slides further confirmed the above observation (Figure 3H). Collectively, these finding
323 confirmed the functional ability of the SAM-RBD and the Circ-RBD vaccines in protecting the
324 mice against SARS-CoV-2 infection.
325
326 **Circ-RBD vaccine formulation is stable in refrigerator (4^0C) and induces a durable**
327 **immune response in both female and male mice**
328 Since Circ-RBD vaccine induced a better overall immune response than the SAM-RBD, we
329 evaluated the stability and durability of the immune response induced by it. To evaluate the
330 effect of prolonged storage (up to 4 weeks) of the Circ-RBD vaccine in the refrigerator (4^0C),
331 it was stored in aliquots in the refrigerator for 2 or 4 weeks, followed by evaluation of its
332 physical and functional characteristics. No change in particle diameter, polydispersity index
333 and percent RNA encapsulation was observed between the samples stored for 2 and 4 weeks,
334 compared to the freshly prepared sample (0 week) (Figures 4A-4C). Mice were injected with
335 aliquots of the same samples in a two-dose immunization schedule (as described above),
336 followed by collection of blood on the 28th day. There was no difference in the anti-RBD IgG
337 titer and the virus neutralization titer (NT_{50}) between freshly prepared and two weeks-stored
338 samples (IgG titer=$2.8X10^5$ and $4X10^5$, NT_{50}=$1.7X10^3$ and $1.3X10^3$ respectively) (Figures 4D
339 and 4E). There was approximately one log drop in the anti-RBD IgG titer and a 1.5 log drop in
340 the virus neutralization titer in the samples stored for 4 weeks at 4^0C (IgG titer=$0.6X10^5$,
341 NT_{50}=$0.04X10^3$) (Figures 4D and 4E).
342 Next, durability of the immune response and influence of gender on the immune response
343 elicited by the Circ-RBD was evaluated by immunizing male and female mice with the Circ-
344 RBD vaccine in a two-dose immunization schedule (day 1 and day 14), followed by
345 measurement of the anti-RBD IgG titer and the virus neutralization titer (NT_{50}) up to 9 months.
346 Both the anti-RBD IgG titer and the virus neutralization titer (NT_{50}) were measured in the mice
347 sera at 1, 3 and 9 months post-first immunization. There was no drop in the anti-RBD IgG titer
348 or the virus neutralization titer (NT_{50}) after 9 months of immunization, with reference to the
349 samples collected after one month of the first immunization (Figures 4F and 4G). Both male
350 and female mice induced a similar level of the anti-RBD IgG titer and the virus neutralization
351 titer (NT_{50}) (Figures 4H and 4I). Collectively, these results demonstrated that Circ-RBD

352 vaccine is stable in standard refrigeration condition and induced a highly durable neutralizing
353 antibody response in both male and female mice.
354
355 **A bivalent SARS-CoV-2 Circ-RBD vaccine induces robust immune response and**
356 **efficiently neutralizes both the Delta and the Omicron BA.1 variant viruses**
357 Recent reports on bivalent mRNA vaccines and nanoparticle vaccine demonstrate their
358 efficacy in conferring broad spectrum immunity against the SARS-CoV-2 variants of concern
359 (Piccoli et al., 2020; Li et al. 2022; Yuan et al., 2022). Feasibility of using the Circ-RNA vaccine
360 technology for developing a bivalent vaccine was tested by evaluating the immunogenicity and
361 virus neutralization potential of a vaccine formulation containing 1:1 mixture of the Circ-RNAs
362 encoding the RBD of the Delta (Circ-RBD^{Del}) and the Omicron BA.1 (Circ-RBD^{Omi}) variants of
363 the SARS-CoV-2. Sequence encoding the RBD region of the Delta and the Omicron variants
364 of the SARS-CoV-2 were inserted into the Circ-RNA backbone vector in place of the RBD
365 (Wuhan) sequence so that both RBD^{Del} and RBD^{Omi} are fused in-frame with the CD5 secretory
366 signal and foldon sequence at their N- and C- terminus, respectively. Expression and secretion
367 of the RBD^{Del} and RBD^{Omi} were verified by western blot analysis of the whole cell lysate and
368 the culture medium of the HEK239T cells transfected with the Circ-RBD^{Del}-LNP and Circ-
369 RBD^{Omi}-LNP formulations. Anti-RBD western blot reveled that both Circ-RBD^{Del} and Circ-
370 RBD^{Omi} were expressed in the HEK239T cells and secreted to the culture medium (Figures
371 5A, upper panel, 5B, upper and middle panel). Secretion of the Circ-RBD^{Omi} was not as
372 efficient as that of the Delta and the Wuhan variants as the ratio of protein in intracellular to
373 culture medium was much higher in the RBD^{Omi} (Figure 5B, middle panel). GAPDH level was
374 measured in aliquots of the same samples to monitor equal loading (Figures 5A, 5B, lower
375 panel). Mice were injected with vaccine formulations containing 10μg of Circ-RBD^{Wuhan}, Circ-
376 RBD^{Del}, Circ-RBD^{Omi} or 1:1 mixture of 5μg Circ-RBD^{Del} and 5ug Circ-RBD^{Omi} in a two-dose
377 immunization schedule at two weeks intervals, as described earlier, followed by collection of
378 blood on day 28 and estimation of the anti-RBD IgG titer and the virus neutralization titer. Mice
379 immunized with the vaccines containing the Circ-RBD^{Wuhan}, Circ-RBD^{Del} and Circ-RBD$^{Del+Omi}$
380 produced an anti-RBD IgG titer of approximately 10^6 against the SARS-CoV-2 Wuhan and
381 Delta variants whereas it was $0.3x10^5$, $0.6x10^5$ and $0.6x10^5$, respectively in case of the
382 Omicron variant (Figures 5C, 5D, 5E). In contrast, the Circ-RBD^{Omi} vaccine induced an
383 average anti-RBD IgG titer of $1.2x10^5$ against the SARS-CoV-2 Wuhan and Delta variants and
384 $1.8x10^5$ against the Omicron variant (Figures 5C, 5D, 5E). The virus neutralization titer (NT_{50})
385 of the sera showed a pattern broadly similar to that of the anti-RBD IgG titer. As observed
386 earlier, NT_{50} of sera from the Circ-RBD^{Wuhan} immunized group against the Wuhan variant was
387 $3.5x10^3$ (Figure 5F). Sera from the Circ-RBD^{Del} and Circ-RBD$^{Del+Omi}$ showed approximately
388 similar NT_{50} as that of the Circ-RBD^{Wuhan} (Figure 5F). However, NT_{50} of sera from the Circ-
389 RBD^{Omi} immunized mice against the Wuhan variant was found to be $0.2x10^3$, which is in line
390 with the data on its anti-RBD IgG titer against the same variant (Figure 5F). NT_{50} of sera from

391 the Circ-RBD^{Del} and the Circ-RBD$^{Del+Omi}$ immunized mice against the SARS-CoV-2 Delta
392 variant was found to be 8.1x10^3 and 8.8x10^3, respectively, indicating that the virus
393 neutralization efficacy of the bivalent vaccine was similar to its monovalent counterparts
394 (Figure 5G). Sera from the Circ-RBD^{Wuhan} immunized mice was almost as efficient as sera
395 from the Circ-RBD^{Del} immunized mice in neutralizing the SARS-CoV-2 Delta variant (NT_{50}=
396 1.7x10^3) (Figure 5G). However, sera from the Circ-RBD^{Omi} immunized mice were significantly
397 less efficient in neutralizing the SARS-CoV-2 Delta variant than that of the Circ-RBD^{Wuhan}, Circ-
398 RBD^{Del} and Circ-RBD$^{Del+Omi}$ immunized mice (Figure 5G). Sera from the Circ-RBD^{Omi} and Circ-
399 RBD$^{Del+Omi}$ immunized mice showed an NT_{50} of 8.1x10^3 and 2.3x10^3, respectively, against the
400 SARS-CoV-2 Omicron BA.1 variant, indicating that bivalent vaccine was equally effective as
401 its monovalent (Circ-RBD^{Omi}) counterpart (Figure 5H). NT_{50} of sera from the Circ-RBD^{Del} and
402 the Circ-RBD^{Wuhan} immunized mice against the Omicron BA.1 variant were found to be 0.3x10^3
403 and 0.06x10^3 respectively, suggesting that they were less efficient in neutralizing the Omicron
404 BA.1 virus (Figure 5H). Collectively, these data demonstrate that the bivalent Circ-RBD
405 vaccine produces potent neutralizing antibodies against the Delta and the Omicron BA.1
406 variants of the SARS-CoV-2.
407

408 **Discussion**

409 With the success of the COVID-19 mRNA vaccines, immunogenicity and protective efficacy
410 of a number of vaccine candidates based on linear mRNAs, self-amplifying mRNAs and
411 circular mRNAs have been evaluated in multiple independent studies. Given their ability to
412 replicate inside the host, SAM RNAs expresses the antigen for a longer duration with lesser
413 amount of the input RNA. Analogous to the SAM-RNA, Circ-RNAs also offer the advantage of
414 expression of the antigen for a longer duration with lesser amount of the input RNA, owing to
415 their higher stability. On top of that, Circ-RNA vaccines do not produce any additional
416 exogenous protein in the target cells, lack open 5'- and 3'-ends and do not produce double
417 strand RNA (dsRNA) in the target cell, all of which are potential unwanted features in the SAM
418 vaccine. Therefore, Circ-RNA vaccines appear to be more promising than the linear mRNA
419 and SAM vaccines. Comparison between linear mRNA and Circ-RNA vaccines have
420 demonstrated the superiority of the later (Qu et al., 2022). However, there are no report on
421 comparison of the protective efficacy between the Circ-RNA and the SAM vaccines. Here, we
422 compared the efficacy of the Circ-RNA and the SAM vaccines by measuring their
423 immunogenicity, virus neutralization potential and protection efficacy using the SARS-CoV-2
424 RBD as the vaccine antigen. After confirming that Circ-RBD vaccine induced a better overall
425 response, we further evaluated its thermostability, longevity of the immune response and
426 compatibility for production of bivalent vaccines.
427 SAM-RNA was produced using the SFV replication machinery. SFV replicon was opted as
428 there are very few reports of SFV infection in human, with very mild symptoms and no
429 instances of mortality. SFV replicon has been used in earlier studies for heterologous protein

430 expression and a recently it has been used to produce a vaccine candidate against the Ebola
431 virus (Liljeström and Garoff, 1991; Krähling et al., 2023). Also note that, multiple outbreaks of
432 VEEV has been reported in North and South American countries with cases of human death.
433 Hence chances of anti-vector immunity is higher in the case of VEEV (Weaver et al., 1996).
434 The Anabaena permuted intron-exon sequence was used to produce the Circ-RNA and CVB3
435 IRES-mediated translation was used to produce the secretory signal and foldon fused-RBD
436 protein in the target cells. Circ-RNA vaccine production using the above vector has been
437 reported and well characterized (Qu et al., 2022). Only the RBD region was used instead of
438 the entire Spike protein of the SARS-CoV-2 as it contains the majority of neutralizing epitopes,
439 avoids induction of antibody-dependent enhancement (ADE) and permits insertion of multiple
440 elements due to its smaller size. The trimeric structure of RBD was maintained using the
441 foldon-motif to improve its immunogenicity and virus neutralization potential, as reported
442 earlier (Routhu et al., 2021).
443 In order to compare the SAM-RBD vaccine with the Circ-RBD vaccine, it was important that
444 both vaccine antigens were expressed at comparable levels and did not induce the host innate
445 immune response. Western blot analysis using anti-RBD antibody and RT-qPCR analysis of
446 the ISGs confirmed that both vaccine candidates expressed similar levels of the vaccine
447 antigen and evaded the host innate immune pathway RNA sensors, respectively.
448 Although both SAM-RBD and Circ-RBD induced a similar humoral response, $CD4^+$ and $CD8^+$
449 memory T cell response was significantly increased in the Circ-RBD immunized mice. There
450 was a trend of increased production of IFNγ and TNFα in CD4+ and CD8+ memory T cells in
451 SAM-RBD immunized mice, however, it was not statistically significant, indicating that Circ-
452 RBD vaccine induced a more potent cell-mediated immune response. SFV replicon system
453 has been used to develop a dual antigen vaccine candidate against the Ebola virus by co-
454 expressing the viral glycoprotein and nucleoprotein where it was observed that high
455 intradermal dose of the Ebola virus glycoprotein induced IFNγ in CD4+ T cells and high
456 intradermal dose of nucleoprotein induced very low level of IFNγ in CD8+ T cells (Krähling et
457 al., 2023). In the case of VEEV-replicon based SARS-CoV-2-RBD and nucleocapsid (N)-
458 expressing dual antigen vaccine immunized outbred mice, IFNγ level was moderately
459 increased in the CD4+ and CD8+ T cells stimulated with either the S- or N-peptide pool
460 (McCafferty et al., 2022). Other studies on evaluation of a SAM vaccine candidate in mice
461 based on the SARS-CoV-2-RBD or the Spike protein expressed from an alpha virus (VEEV/
462 VEEV+Sindbis) replicon reported a significant T- cell response in splenocytes of the
463 immunized mice, upon stimulation with the S-peptide pool (McKay et al., 2020; Erasmus et al.,
464 2020; de Alwis et al., 2021; Maruggi et al., 2022). However, SAM-Spike immunized pigtail
465 macaques did not induce high level of IFNγ production in CD4+ and CD8+ T cells upon
466 stimulation of splenocyte with S-peptide pool (Erasmus et al., 2020). On the other hand, the
467 Circ-RBD vaccine of the SARS-CoV-2 induced similar level of T cell response as that of the
468 corresponding linear mRNA vaccine and a higher neutralizing antibody response than that of

469 the linear mRNA (Qu et al., 2022). Given that different assays were conducted in different
470 laboratories to measure the T cell response, it is possible that lower IFNγ and TNFα production
471 in CD4+ and CD8+ T cells (splenocytes stimulated with RBD peptide pool) may be attributed
472 to the overall lesser sensitivity of our assay protocol. However, the relative difference in the
473 level of IFNγ and TNFα between SAM-RBD and Circ-RBD immunized sample would remain
474 constant as the samples were processed in parallel. Therefore, Circ-RBD vaccine appears to
475 be a better alternative to a SAM-RBD vaccine. Whether a VEEV replicon-based SAM vaccine
476 shows a similar profile as the SFV replicon used in our study, remains to be tested. A recent
477 study also showed potent adjuvant function of the circular RNA, irrespective of the antigen
478 sequence and robust CD8+ T-cell response induced by a circular RNA vaccine encoding the
479 nucleoprotein of the influenza virus, further supporting practical utility of the circular RNA
480 vaccine technology (Amaya et al., 2023).
481 Functional efficacy of the Circ-RBD vaccine was characterized by evaluating its
482 thermostability, durability of the neutralizing antibody response, ability to protect the mice upon
483 SARS-CoV-2 challenge and compatibility as a bivalent vaccine formulation. Circ-RBD
484 immunization induced peak anti-RBD IgG titer at 4 weeks, which protected the mice from
485 COVID-19 like disease pathology when SARS-CoV-2 infection was initiated in the lower
486 respiratory tract (severe disease, often leading to lethality). Nine month follow up study of the
487 anti-RBD IgG titer and the virus neutralization titer (NT_{50}) did not show any decline in both.
488 Moreover, neutralizing antibody titer was similar in both male and female mice. With regard to
489 stability of the Circ-RBD vaccine in normal refrigeration conditions, there was no change in
490 the characteristic of the Circ-RBD-LNP formulation after 4 weeks of storage, however
491 neutralizing antibody titer was stable for up to 2 weeks of storage. Finally, we evaluated the
492 functional efficacy of a bivalent Circ-RBD vaccine. Failure of monovalent vaccines in
493 preventing COVID-19 for a longer period is ascribed to emergence of newer variants of the
494 SARS-CoV-2 containing escape mutations in the RBD region. Bivalent vaccines based on
495 linear mRNA platform or nanoparticle platform expressing the spike protein or RBD region of
496 the spike protein of the SARS-CoV-2-Delta and Omicron variants have shown cross-protection
497 against SARS-CoV-2 variants (Corleis et al., 2023; Li et al., 2022; Yuan et al. 2022). On similar
498 line, our data on the bivalent Circ-RBD vaccine expressing the RBD of Delta and Omicron
499 variants demonstrate cross-protection against the Wuhan, Delta and Omicron variants.
500 In summary, the current study compared the immunogenicity and virus neutralization efficacy
501 of the SAM and Circ-RNA vaccine candidates encoding the SARS-CoV-2-RBD antigen, which
502 revealed similar humoral immune response and virus neutralization potential of both vaccines
503 and a superior cell-mediated immune response induced by the later. Our data also showed
504 reasonable stability of the Circ-RNA vaccine at four degrees centigrade, high durability of the
505 neutralizing antibody response induced by it and high virus neutralization efficacy of the
506 bivalent Circ-RNA vaccine, all of which support the use of Circ-RNA technology in vaccine
507 development. An earlier study showed the superiority of the SARS-CoV-2 Circ-RNA vaccine

508 over the corresponding linear mRNA vaccine. Data obtained from this study further supports
509 the use of the Circ-RNA technology for vaccine development.
510

511 **Materials and Methods:**

512 **Plasmids and reagents**

513 Plasmid encoding the noninfectious Semliki Forest virus replicon (pSFV3) was a gift from
514 Henrik Garoff (Addgene plasmid # 92072 ; http://n2t.net/addgene:92072 ;
515 RRID:Addgene_92072) (Liljeström and Garoff, 1991). 988 to 1578 nucleotides encoding the
516 RBD region (330 to 526 amino acids) of spike protein of the SARS-CoV-2 Wuhan isolate
517 (hCoV-19/USA-WA1/2020) fused in-frame with the CD5 secretory sequence at the N-terminal
518 and the Bacteriophage T4 fibritin trimerization motif sequence at the C-terminus was
519 synthesized and inserted into the pSFV3 vector at the BamH1 restriction site. The resulting
520 plasmid was named pSFV3-RBD. Transcription of SFV-RBD hybrid RNA in the pSFV3-RBD
521 vector was under control of the SP6 promoter. A circular RNA expression cassette containing
522 the sequence of the T7 promoter, Anabaena Group 1 intron 3' sequence, CVB3 IRES
523 sequence, CD5 secretory sequence, RBD region (988 to 1578 nucleotides) of spike protein of
524 the SARS-CoV-2 Wuhan isolate (hCoV-19/USA-WA1/2020), bacteriophage T4 fibritin
525 trimerization motif and anabaena group 1 intron 5' sequence was chemically synthesised in
526 the given order and cloned into the pUC57 vector. The resulting plasmid was named pUC57
527 cRNA-RBD^{Wuhan}. RBD corresponding to the SARS-CoV-2-Delta (hCoV-19/USA/MD-
528 HP05285/2021) and Omicron (hCov-19/USA/MD-HP2087/2021) variants were cloned
529 similarly and the resulting plasmids were named pUC57 cRNA-RBD^{Del} and pUC57 cRNA-
530 RBD^{Omi}, respectively. The goat anti-Mouse IgG-HRP (Catalog No. 1030-05) was from
531 Southern Biotech (Alabama, USA). Megascript SP6 transcription kit (Catalog no. AM1330),
532 MegaScript T7 transcription kit (Catalog no. AM1334) lipofectamine 3000 (Catalog No.
533 L3000075), anti-SARS-CoV-2 Spike S1 (Catalog no. PA5-81795), goat anti-Rabbit IgG-HRP
534 (Catalog No. 31460), Anti-mouse IgG (H+L) Alexa Flour 488 (Catalog no. A28175) and
535 Ribogreen (Catalog no. R11490) were from Thermo Fisher Scientific (Massachusetts, USA).
536 Scriptcap Cap 1 capping system (Catalog no. sccs1710) was from CellScript (Wisconsin,
537 USA). RNAse R (Catalog no. ab286929) was from Abcam (Cambridge, United Kingdom).
538 RNeasy Kit was from Qiagen ((Catalog no. 74104, Hilden, Germany). SM102 (Catalog no.
539 33474) was from Cayman Chemical company (Michigan, USA). DSPC (Catalog no. 850365P),
540 Cholesterol (Catalog no. 700000P), and DMG-PEG 2000 (catalog no. 880151P), was from
541 Sigma (Missouri, USA). Amicon ultra centrifugal filter (Catalog no. UFC703008) was from
542 Merck Millipore (Darmstadt, Germany). anti-GAPDH antibody (Catalog no. SC-25778) was
543 from Santa Cruz Biotechnology (Texas, USA). TRI-reagent (Catalog no. TR118) was from
544 MRC (Massachusetts, USA). Firescript cDNA synthesis kit (Catalog no. 06-15-00050) and
545 HOT FIREPol SolisGreen qPCR Mix (Catalog no.08-47-0000S) from Solis Biodyne (Estonia).
546 Ad5-hACE (catalog no. VVC-McCray-7723) was obtained from the Viral Vector Core

547 (University of Iowa, Iowa, USA). Vetbond (catalog no. 1469Sb) was from 3M (Minnesota,
548 USA). Mouse monoclonal antibody isotyping reagent (Cat no. ISO2) was from Sigma Aldrich
549 (Missouri, USA). SARS-CoV-2 spike antibody (catalog no. GTX632604) was from GeneTex
550 (California, USA). SARS-CoV-2 RBD peptide pool (Catalog no: PM-WCPV-S_RBD-1) was
551 from JPT innovative peptide solution (Berlin, Germany). GolgiStop (Catalog no. 554724) was
552 from BD bioscience (New Jersey, USA). FC (Catalog no.14-9161-73), IC fixation buffer
553 (Catalog no. FB001), permeabilizing buffer (Catalog no. 00-8333-56), anti-mouse CD3
554 (Catalog no.100204), anti-mouse CD4 (Catalog no.100408), anti-mouse CD8 (Catalog
555 no.100714), anti-mouse CD44 (Catalog no.103030), anti-mouse IFNγ (Catalog no. 505810),
556 TNFα (Catalog no. 506328), and IL-4 (Catalog no. 504126) are from Thermo Fisher Scientific
557 (Massachusetts, USA).
558
559 ***In vitro* transcription, capping, circularization, RNase R treatment and purification**
560 pSFV3-RBD, pUC57 cRNA-RBD^{Wuhan}, pUC57 cRNA-RBD^{Del} and pUC57 cRNA-RBD^{Omi}
561 plasmids were linearized and purified DNA was used for the *in vitro* transcription using the
562 Megascript SP6 or T7 transcription kit, following the manufacturer's instruction. SAM-RNA was
563 capped using the Scriptcap Cap 1 capping system, following the manufacturer's instructions.
564 In the case of Circ-RNA, *in vitro* transcribed RNA was incubated at 55^{0}C for 15 min in the
565 circularization buffer (10mM $MgCl_2$, 50mM Tris-HCl, 100mM NaCl, 1mM DTT, pH 7.9; New
566 England Biolabs, USA) and 2μM rGTP to circularize the RNA, as described earlier
567 (Wesselhoeft et al., 2018b). Circularized RNA was incubated at 37^{0}C for 7 min with 0.1units
568 RNase R/μg RNA, followed by addition of 0.1 units RNase R/μg RNA and incubation for
569 another 7 min. RNA was purified using the RNeasy kit, following the manufacturer's protocol
570 (Qiagen, Germany).
571
572 **Preparation and characterization of the RNA-LNP vaccine formulation,**
573 SM102, DSPC, Cholesterol and DMG-PEG 2000 were mixed at a molar ratio of 50:10:38.5:1.5
574 in absolute ethanol at 1/5 of the final LNP amount. An aqueous solution of RNA was prepared
575 by diluting it in 50mM acetate buffer (1.2mM sodium acetate, 4mM acetic acid, pH 4.0) at 4/5
576 of the final LNP volume. The two solutions were mixed using a microfluidics system (ElveFlow
577 Elvesys, France) at a flow rate ratio of 1:5. The resulting RNA-LNP complex was dialyzed with
578 phosphate buffered saline (137 mM NaCl, 2.7 mM KCl, 10 mM Na_2HPO_4, 1.8 mM KH_2PO_4,
579 pH 6.8) and concentrated using a 30kDa MWCO Amicon ultra centrifugal filter to a volume of
580 0.1μg/μl RNA concentration. Further, the RNA-LNP vaccine formulation was passed through
581 a 0.2μm filter and aliquoted into glass vials and stored at 4^{0}C. Size and polydispersity (PDI) of
582 the RNA-LNP vaccine formulation was evaluated by dynamic light scattering (ZetaSizer lab,
583 Malvern panalytical, United Kingdom). For transmission electron microscopy (TEM), RNA-
584 LNP vaccine formulation was diluted ten times in H_2O, followed by staining with 2% uranyl
585 acetate and image acquisition using JEM-1400 Flash TEM equipped with tungsten filament

586 and sCMOS camera (JEOL Ltd, Japan). RNA encapsulation into LNP was measured by
587 fluorescent-based RNA quantification system using Ribogreen, following manufacturer's
588 instruction. The encapsulated RNA was released from the LNP by treating the RNA-LNP
589 vaccine formulation with 2% Triton X-100, followed by measurement of RNA quantity by
590 Ribogreen assay and evaluation of RNA quality by agarose gel electrophoresis.
591
592 **Mammalian cell culture, transfection, western blot, RT-qPCR, SARS-CoV-2 propagation**
593 HEK293T cells were maintained in Dulbecco's modified Eagle medium (DMEM)
594 supplemented with 10% FBS (fetal bovine serum) and Penicillin, Streptomycin during
595 maintenance. Cells were seeded on 6 well plates ($8x10^5$ cell/well) and transfected with 6μg
596 of RNA-LNP complex. Only LNP was added in the mock. For western blot analysis under
597 reducing condition, samples (cells or culture medium) were incubated at 95^0C for 5 minutes
598 in Laemlli buffer (2% SDS, 13% glycerol, 2.5% β-mercaptoethanol, 0.005% bromo phenol
599 blue and 63 mM Tris HCl, pH 6.8). For non-reducing condition, β-merceptoethanol was
600 omitted from the Laemlli buffer. Total protein in the samples was quantified by Bicinchoninic
601 acid assay and equal amount of protein were resolved in SDS-PAGE, followed by transfer to
602 Polyvinylidene fluoride (PVDF) membrane. The membrane was blocked with 5% skimmed
603 milk, incubated with anti-Spike S1 or anti-GAPDH antibody at 1:5000 dilution. Anti-Rabbit
604 secondary antibodies (Santa Cruz Biotechnology) were used at 1:5000 dilution. Protein
605 bands were developed by enhanced chemiluminescence reagent, using a commercially
606 available kit (BioRad, USA) and visualized in a gel Documentation system (Chemidoc MP,
607 Bio Rad, USA).
608 For RT-qPCR analysis of genes involved in the antiviral response pathway, HEK293T cells
609 were transfected with 1μg of SAM-RBD or Circ-RBD RNA or Poly I:C was using lipofectamine
610 3000, following manufacturer's instruction (Thermo Fisher Scientific, Massachusetts, USA).
611 24 hours post-transfection, total RNA was isolated using the TRI-reagent (MRC,
612 Massachusetts, USA), followed by reverse transcription (RT) using the Firescript cDNA
613 synthesis kit (Solis Biodyne, Estonia). The relative transcript levels of different genes were
614 determined by SYBR green based RT-qPCR, as described earlier (Verma et al., 2021). Values
615 obtained for GAPDH RNA was used as an internal control for normalization of the data. Primer
616 sequences are as follows: hGAPDH FP: 5' GAGTCAACGGATTTGGTCGT 3', hGAPDH RP:
617 5' TTGATTTTGGAGGGATCTCG 3', hIFNβ FP: 5' ACGCCGCATTGACCATCTAT 3', hIFNβ
618 RP: 5' TTGGCCTTCAGGTAATGCAGA 3', hRIG-I FP: 5' TGTGGGCAATGTCATCAAAA 3',
619 hRIG-I RP: 5' GAAGCACTTGCTACCTCTTGC 3', hOASL FP; 5'
620 AGGGTACAGATGGGACATCG 3', hOASL RP: 5' AAGGGTTCACGATGAGGTTG 3', hPKR
621 FP: 5' TCTTCATGTATGTGACACTGC 3', hPKR RP: 5' CACACAGTCAAGGTCCTT 3',
622 hOAS1 FP: 5' GCTCCTACCCTGTGTGTGTGT 3', hOAS1 RP: 5'
623 TGGTGAGAGTACTGAGGAAGA 3'.

624 For RT-qPCR analysis in the mouse lung tissue, total RNA was isolated from 10mg lung tissue
625 using TRI reagent, following manufacturer's instruction. cDNA synthesis and RT-qPCR was
626 done as mentioned above. HPRT RNA level was quantified for normalization of data. Primer
627 sequences are as follows: SCoV2 FP: 5' TGGACCCCAAAATCAGCGAA 3', SCoV2 RP: 5'
628 TCGTCTGGTAGCTCTTCGGT 3', mHPRT FP: 5' GTTGGATACAGGCCAGACTTTGTTG 3',
629 mHPRT RP: 5' GATTCAACTTGCGCTCATCTTAGGC 3', mIL-6 FP: 5'
630 GAGGATACCACTCCCAACAGACC 3', mIL-6 RP: 5' AAGTGCATCATCGTTGTTCATACA 3',
631 mIL-1β FP: 5' GCCCATCCTCTGTGACTCAT 3', mIL-1β RP: 5'
632 AGGCCACAGGTATTTTGTCG 3', mTNFα FP: 5' CATCTTCTCAAAATTCGAGTGACAA 3',
633 mTNFα RP: 5' TGGGAGTAGACAAGGTACAACCC 3', mIFNγ FP: 5'
634 AACGCTACACACTGCATCTTGG 3', mIFNγ RP: 5' GACTTCAAAGAGTCTGAGG 3'.
635 SARS-CoV-2 Wuhan isolate (NR-52281, SARS-related coronavirus-2 isolate ISA-WA1/2020)
636 and Omicron Variants (B.1.1.529, NR56461, SARS-related coronavirus-2 isolate hCoV-
637 19/USA/MD-HP20874/2021) were obtained from BEI Resources, amplified in Vero E6 cells in
638 the BSL3 facility of THSTI, India, titrated and stored frozen in aliquots. SARS-CoV-2-Delta
639 (SARS-CoV-2/human/IND/THSTI_287/2021) was isolated from clinical sample at THSTI and
640 has been reported (GenBank: MZ356566.1). SARS-CoV-2 infection was done as described[43].
641

642 **Mice handling, immunization, SARS-CoV-2 challenge study**

643 Mice were housed in individually ventilated cages at the experimental animal facility of THSTI.
644 For SARS-CoV-2 infection experiments, animals were housed in the animal biosafety level-3
645 (ABSL-3) laboratory of THSTI. Institutional animal ethics committee and institutional biosafety
646 committee approval was obtained for the experiments. Male and Female Balb/c mice of 6 to
647 8 weeks old were intradermally injected on the back of the animal. In the case of intramuscular
648 injection, mice were injected in the hind leg muscle. All injections were in 100μl volume.
649 Placebo animal received 100μl PBS. Blood was collected at the indicated time points through
650 retro-orbital sinus using a sterile hematocrit capillary tube. Wherever indicated, mice were
651 euthanized by anesthetic overdose (Ketamine 300 mg/kg and xylazine 30 mg/kg) and blood,
652 spleen and lungs were collected. Serum was isolated from the blood by centrifugation at
653 10,000g for 10 min at 4°C. Lung tissue was cut into parts and used for RNA, protein or
654 histopathology analysis.
655 SARS-CoV-2 challenge experiments were conducted in inbred Balb/c mice. Six to eight-week-
656 old mice were immunized with 10μg of Circ-RBD twice at two-weeks interval. Blood was
657 collected through retro-orbital sinus and anti-RBD IgG was measured. Replication deficient
658 adenovirus expressing human ACE2 (Ad5CMV-hACE2, denoted as hACE2) was transduced
659 through intranasal or intratracheal route (Hassan et al., 2020; Gu et al., 2021). For Intranasal
660 transduction, mice were lightly anaesthetized with isoflurane and $2x10^8$ pfu of hACE2 was
661 administered, as described (Hassan et al., 2020). Intratracheal transduction of hACE2 was
662 performed as described (Gu et al., 2021). Mice were anaesthetised with ketamine xylazine

663 injection (Ketamine 100 mg/kg and xylazine 10 mg/kg), hair was shaved from the neck region
664 and a 5mm incision was made in the skin to expose the trachea. $2x10^8$ pfu of hACE2 was
665 administered in the trachea using a 24-gauge I.V. cannula. The wound opening was glued
666 with tissue adhesive (Vetbond, 3M Corp, USA). Animals did not show any sign of illness or
667 inflammation at the site of glue. Mice were infected with 10^5 pfu SARS-CoV-2 intranasally after
668 5 days of hACE2 administration. Weight of the animals were measured before infection and
669 every day after the infection. In the intranasal transduction model, mice were sacrificed 5 days
670 post-SARS-CoV-2 infection and lung and BAL fluid were harvested. In the case of intratracheal
671 transduction model, weight was measured every day after infection and survival was checked
672 till 21 days of post-infection. When an animal showed critical illness symptoms after SARS-
673 CoV-2 infection, it was euthanized and samples were collected. An animal from the immunized
674 group was euthanized for comparison when mice from the placebo group were euthanized.
675
676 **ELISA, Flow cytometry, quantification of viral load, virus Neutralization assay,**
677 The Enzyme-Linked Immunosorbent Assay (ELISA) was performed as described, with below
678 mentioned modifications (Mehdi et al., 2021). The receptor-binding domains (RBDs) of the
679 three SARS-CoV-2 variants-Wuhan, Delta, and Omicron, were expressed in-house in the
680 Expi293 cells (Thermo Fisher Scientific, Massachusetts, USA) and used in the ELISA. The
681 assay samples (mice sera) were diluted in a 3-fold series from 1:500 to 1:1,093,500. Horse
682 radish peroxidase (HRP)-labelled Goat anti-Mouse IgG (H+L) (Jackson ImmunoResearch,
683 USA) was used at a dilution of 1:5000. The endpoint anti-RBD IgG titer (denoted as anti-RBD
684 IgG titer in the text and figures) refers to the dilution factor at which the absorbance (obtained
685 in the ELISA) of the test samples exceeded three times that of the background (secondary
686 Ab alone). Anti-RBD IgM and IgG isotype (IgG1, IgG2a and IgG2b) ELISA was performed
687 using a commercially available kit, following the manufacturer protocol (Sigma Aldrich) at a
688 serum dilution of 1:500.
689 For FACS study, splenocytes were prepared as described and cultured in RPMI-10
690 supplemented with 10%fetal bovine serum and 1% penicillin-streptomycin antibiotic (Agarwal
691 et al., 2022). After 3 hours, RBD peptide pool (2 μg/ml each peptide) and GolgiStop (BD) was
692 added to the culture medium for 6 hours. Cells were blocked with FC at room temperature for
693 15 min, stained with anti-CD3, anti-CD4, anti-CD8 and anti-CD44 antibodies followed by
694 fixation and permeabilization. Intracellular staining of IFNγ, TNFα and IL-4 was performed
695 using respective antibodies. Cells were sorted using the BD FACS-aria (BD Biosciences) and
696 data was analyzed using the FlowJo software (FlowJo LLC, Oregon, USA).
697 For quantification of SARS-CoV-2 level in the lungs, 5mg of lung tissue was homogenised in
698 1ml serum free DMEM and sterilized using 0.2μm filter. The homogenate was serially diluted
699 10-fold and added to $2x10^5$ VeroE6 cells/well in 12 well plate for 1 hour. Infection medium was
700 removed, 1% carboxymethyl cellulose (CMC) was added and plates were incubated for 48
701 hours at 37^0C, with 5% CO_2 supplementation. Cells were fixed in 3.7% formaldehyde for

702 overnight, plaques stained with 0.05% crystal violet and number of plaques in each well was
703 counted.
704 50% virus neutralization efficiency (NT_{50}) of the sera from mice immunized with the SAM-
705 RBD^{Wuhan} and Circ-RBD^{Wuhan} vaccine formulations (shown in Figs. 2D, 3E, 3F, 3H, 3J, S1B
706 and S1D) were measured by the Plaque reduction neutralization test (PRNT), as described
707 (Bewley et al., 2021). Briefly, mouse sera were heated at 55^0C for 30 min, 2-fold serially
708 diluted starting from 1:10 in serum-free DMEM, mixed with an equal volume of virus [virus
709 stock was appropriately diluted so that each well produces approximately 50 plaque forming
710 units (pfu)] and incubated at 37^0C for 1 hour. $2x10^5$ VeroE6 cells/well in 12 well plates were
711 incubated with the serum-virus mix for 1 hour. Infection medium was removed and cells
712 were overlaid with 1% CMC in 2% FBS supplemented DMEM and incubated at 37^0C with
713 5%CO_2 supplementation for 48 hours. Cells were fixed in 3.7% formaldehyde for overnight
714 and stained with 0.2% crystal violet. The number of plaques were counted and the serum
715 dilution leading to 50% neutralization of the virus (NT_{50}) was calculated using the GraphPad
716 Prism 9.0 (Massachusetts, USA). NT_{50} of the Wuhan, Delta and Omicron variants (shown in
717 Figures 6F-6H) were measured by the Focus reduction neutralization test (FRNT). Heat
718 inactivated serum sample were 2- fold serially diluted, starting from 1:20 and mixed with an
719 equal volume of the virus [virus stock was appropriately diluted so that each well produces
720 approximately 100 focus forming units (ffu)] and incubated at 37^0C for 1 hour. $2x10^4$ VeroE6
721 cells/well in 96 well plates were incubated with the serum-virus mix for 1 hour. Infection
722 medium was removed and cells were overlaid with 0.5% CMC in 2% FBS supplemented
723 DMEM and incubated at 37^0C with 5%CO_2 supplementation for 24 hours. Cells were fixed in
724 formaldehyde and permeabilized with 0.2% Triton X-100. Next, the cells were stained with
725 anti-Spike antibody, following manufacturer's protocol followed by staining with alexa fluor-
726 488-conjugated anti-mouse IgG antibody. The number of foci was counted using an
727 ELISPOT reader (iSPOT, AID GmBh, Strassberg, Germany) and the serum dilution leading
728 to 50% neutralization of the virus was calculated using GraphPad Prism 9.0.

729 **Histopathology**

730 Histopathology analysis of the lung tissue samples were performed by the histology service of
731 the experimental animal facility of THSTI, following established protocol. Briefly, lung
732 tissues were kept in 10% neutral buffered formalin solution immediately after collection. After
733 ensuring proper fixation, samples were subjected to processing and paraffin embedded blocks
734 were prepared. 4μm thick sections were cut using a semi-automatic microtome (Histocore
735 Multicut- Leica Biosystem, Germany) and mounted on glass slides. The sections were stained
736 with haematoxylin and eosin, following standard operating procedures of the facility. Slides
737 were analysed by a qualified histopathologist, following blind evaluation method. Semi-
738 quantitative scoring system was adopted to score the pathological conditions, 0 indicating
739 absence of a pathological condition while 5 indicating its highest severity. Pathological

conditions such as; bronchiolitis, vasculitis, interstitial pneumonia, alveolitis and haemorrhage were analysed and scored. Images were visualized and captured using a Bright field upright microscope (CX43RF- Olympus Life science Solutions, Japan) equipped with a colour camera (DP28- Olympus Life science Solutions, Japan) and imaging software (cellSens Entry- Olympus Life science Solutions, Japan) at 200X magnification.

Statistical analysis

All cell line data are derived from 3 independent experiments and represented as mean±SD of 3 independent experiments. For mouse study, 6 or more animals were used in each group, as indicated in the figures. Average values are shown in the bar and individual values are shown as dots in each bar in the graphs. Two-tailed unpaired t-test (Mann-Whitney) and One-way ANOVA (Kruskal-Wallis test) followed by Dunn's multiple comparisons was used for comparison between groups, as indicated in the figures. Logistic regression was used to determine the NT_{50} titre of the mice sera. All statistical analysis was performed using the GraphPad Prism 9. A *p*-value <0.05 with 95% confidence interval was considered statistically significant.

Acknowledgement

This study was partly supported by a BIRAC (Biotechnology Industry Research Assistance Council, Department of Biotechnology, Government of India) grant to MS (BT/COVID0081/01/20) and THSTI core grant to MS. ONS and UB are supported by senior research fellowships from the Council of scientific and industrial research and the department of Biotechnology, Government of India, respectively. We are thankful to the experimental animal facility and biosafety level three (BSL3) facility of THSTI for helping with the experiments. The following reagent was deposited by the Centre for Disease Control and Prevention (USA) and obtained through BEI Resources, NIAID, NIH (USA): SARS-Related Coronavirus 2, isolate hCoV-19/USA-WA1/2020, NR-52281 and SARS-Related Coronavirus 2, isolate hCoV-19/USA/MD-HP20874/2021 (Lineage B.1.1.529; Omicron Variant), NR-56461, contributed by Andrew S. Pekosz. We are thankful to Henrik Garoff for the pSFV3 plasmid.

Author contribution

Conceptualization: MS; Investigation: ONS, UB, GJ, TRA, KC, SN, PS, SC, FM; Data analysis: ONS, GJ, TRA, BNP, SM, GB, CTRK, PG, MS; Resources: TS, SM, DN, GB, CTRK, PG, MS; manuscript writing: ONS, MS, GB, SM, CTRK. All authors have reviewed, edited and agreed to the final version of the manuscript.

Declaration of interest

The authors have no conflict of interest to declare.

Keywords: SARS-CoV-2, mRNA vaccine, self-amplifying mRNA, Circular mRNA, COVID-19, SARS-CoV-2 vaccine.

Reference

Agarwal, S., Kaur, S., Asuru, T.R., Joshi, G., Shrimali, N.M., Singh, A., Singh, O.N., Srivastva, P., Shrivastava, T., Vrati, S., et al. (2022). Dietary alpha-ketoglutarate inhibits SARS CoV-2 infection and rescues inflamed lungs to restore O(2) saturation by inhibiting pAkt. Clin. Transl. Med. 12, e1041. https://doi.org/10.1002/ctm2.1041.

Amaya, L., Grigoryan, L., Li, Z., Lee, A., Wender, P.A., Pulendran, B., Chang, H.Y. (2023). Circular RNA vaccine induces potent T cell responses. Proc. Natl. Acad. Sci. USA 120, e2302191120. https://doi.org/10.1073/pnas.2302191120.

Arevalo, C.P., Bolton, M.J., Le Sage, V., Ye, N., Furey, C., Muramatsu, H., Alameh, M.G., Pardi, N., Drapeau, E.M., Parkhouse, K., et al. (2022). A multivalent nucleoside-modified mRNA vaccine against all known influenza virus subtypes. Science 378, 899-904. https://doi.org/10.1126/science.abm0271.

Baden, L.R., El Sahly, H.M., Essink, B., Kotloff, K., Frey, S., Novak, R., Diemert, D., Spector, S.A., Rouphael, N., Creech, C.B., et al. (2021). Efficacy and safety of the mRNA-1273 SARS-CoV-2 vaccine. N. Engl. J. Med. 384, 403-416. https://doi.org/10.1056/NEJMoa203538.

Bewley, K.R., Coombes, N.S., Gagnon, L., McInroy, L., Baker, N., Shaik, I., St-Jean, J.R., St-Amant, N., Buttigieg, K.R., Humphries, H.E., et al. (2021). Quantification of SARS-CoV-2 neutralizing antibody by wild-type plaque reduction neutralization, microneutralization and pseudotyped virus neutralization assays. Nat. Protoc. 16, 3114-3140. https://doi.org/10.1038/s41596-021-00536-y.

Bloom, K., van den Berg, F., Arbuthnot, P. (2021). Self-amplifying RNA vaccines for infectious diseases. Gene therapy 28, 117-129. https://doi.org/10.1038/s41434-020-00204-y.

Breuer, J., Barth, P., Noe, Y., Shalamova, L., Goesmann, A., Weber, F. and Rossbach, O. (2022). What goes around comes around: Artificial circular RNAs bypass cellular antiviral responses. Mol. Ther. Nucleic Acids 28, 623-635. https://doi.org/10.1016/j.omtn.2022.04.017.

Cameroni, E., Bowen, J.E., Rosen, L.E., Saliba, C., Zepeda, S.K., Culap, K., Pinto, D., VanBlargan, L.A., De Marco, A., di Iulio, J., et al. (2022) Broadly neutralizing antibodies overcome SARS-CoV-2 Omicron antigenic shift. Nature 602, 664-670. https://doi.org/10.1038/s41586-021-04386-2.

Carabelli, A.M., Peacock, T.P., Thorne, L.G., Harvey, W.T., Hughes, J., Peacock, S.J., Barclay, W.S., De Silva, T.I., Towers, G.J., et al. (2023). SARS-CoV-2 variant biology: immune escape, transmission and fitness. Nat. Rev. Microbio. 21, 162-177. https://doi.org/10.1038/s41579-022-00841-7.

Chaudhary, N., Weissman, D., Whitehead, K.A. (2021). mRNA vaccines for infectious diseases: principles, delivery and clinical translation. Nat. Rev. Drug Discov. 20, 817-838. https://doi.org/10.1038/s41573-021-00283-5.

Corleis, B., Hoffmann, D., Rauch, S., Fricke, C., Roth, N., Gergen, J., Kovacikova, K., Schlottau, K., Halwe, N.J., Ulrich, L., et al. (2023) Efficacy of an unmodified bivalent mRNA vaccine against SARS-CoV-2 variants in female small animal models. Nat. Commun. 14, 816. https://doi.org/10.1038/s41467-023-36110-1.

De Alwis, R., Gan, E.S., Chen, S., Leong, Y.S., Tan, H.C., Zhang, S.L., Yau, C., Low, J.G., Kalimuddin, S., Matsuda, D., et al. (2021). A single dose of self-transcribing and replicating RNA-based SARS-CoV-2 vaccine produces protective adaptive immunity in mice. Mol. Ther. 29, 1970-1983. https://doi.org/10.1016/j.ymthe.2021.04.001.

Erasmus, J.H., Khandhar, A.P., O'Connor, M.A., Walls, A.C., Hemann, E.A., Murapa, P., Archer, J., Leventhal, S., Fuller, J.T., Lewis, T.B., et al. (2020). An Alphavirus-derived replicon RNA vaccine induces SARS-CoV-2 neutralizing antibody and T cell responses in mice and nonhuman primates. Sci. Transl. Med. 12, eabc9396. https://doi.org/10.1126/scitranslmed.abc9396.

Gu, T., Zhao, S., Jin, G., Song, M., Zhi, Y., Zhao, R., Ma, F., Zheng, Y., Wang, K., Liu, H., et al. (2020). Cytokine Signature Induced by SARS-CoV-2 Spike Protein in a Mouse Model. Front. Immunol. 11, 621441. https://doi.org/10.3389/fimmu.2020.621441.

Hassan, A.O., Case, J.B., Winkler, E.S., Thackray, L.B., Kafai, N.M., Bailey, A.L., McCune, B.T., Fox, J.M., Chen, R.E., Alsoussi, W.B., et al. (2020). A SARS-CoV-2 Infection Model in Mice Demonstrates Protection by Neutralizing Antibodies. Cell 182, 744-753. https://doi.org/10.1016/j.cell.2020.06.011.

Heine, A., Juranek, S., Brossart, P. (2021).Clinical and immunological effects of mRNA vaccines in malignant diseases. Mol. Cancer 20, 52. https://doi.org/10.1186/s12943-021-01339-1.

Karikó, K., Muramatsu, H., Welsh, F.A., Ludwig, J., Kato, H., Akira, S., Weissman, D., (2008). Incorporation of pseudouridine into mRNA yields superior nonimmunogenic vector with increased translational capacity and biological stability. Mol. Ther. 16, 1833-1840. https://doi.org/10.1038/mt.2008.200.

Krähling, V., Erbar, S., Kupke, A., Nogueira, S.S., Walzer, K.C., Berger, H., Dietzel, E., Halwe, S., Rohde, C., Sauerhering L., et al. (2023). Self-amplifying RNA vaccine protects mice against lethal Ebola virus infection. Mol. Ther. 31, 374-386. https://doi.org/10.1016/j.ymthe.2022.10.011.

Krienke, C., Kolb, L., Diken, E., Streuber, M., Kirchhoff, S., Bukur, T., Akilli-Öztürk, Ö., Kranz, L.M., Berger, H., Petschenka, J., et al.(2021). A noninflammatory mRNA vaccine for treatment of experimental autoimmune encephalomyelitis. Science 371, 145-153. https://doi.org/10.1126/science.aay3638.

Li, J., Liu, Q., Liu, J., Fang, Z., Luo, L., Li, S., Lei, Y., Li, Z., Jin, J., Xie, R., et al. (2022) Development of Bivalent mRNA Vaccines against SARS-CoV-2 Variants. Vaccines (Basel) 10. https://doi.org/10.3390/vaccines10111807.

Liljeström, P., Garoff, H. (1991). A new generation of animal cell expression vectors based on the Semliki Forest virus replicon. Nat. Biotech. 9, 1356-1361. https://doi.org/10.1038/nbt1291-1356.

Liu, C.X., Chen, L.L. (2022). Circular RNAs: Characterization, cellular roles, and applications. Cell 185, 2016-2034. https://doi.org/10.1016/j.cell.2022.04.021.

Liu, L., Iketani, S., Guo, Y., Chan, J.F.W., Wang, M., Liu, L., Luo, Y., Chu, H., Huang, Y., Nair, M.S., et al. (2022). Striking antibody evasion manifested by the Omicron variant of SARS-CoV-2. Nature 602, 676-681. https://doi.org/10.1038/s41586-021-04388-0.

Maruggi, G., Mallett, C.P., Westerbeck, J.W., Chen, T., Lofano, G., Friedrich, K., Qu, L., Sun, J.T., McAuliffe, J., Kanitkar, A., et al. (2022). A self-amplifying mRNA SARS-CoV-2 vaccine candidate induces safe and robust protective immunity in preclinical models. Mol. Ther. 30, 1897-1912. https://doi.org/10.1016/j.ymthe.2022.01.001.

McCafferty, S., Haque, A.A., Vandierendonck, A., Weidensee, B., Plovyt, M., Stuchlíková, M., François, N., Valembois, S., Heyndrickx, L., Michiels, J., et al. (2022). A dual-antigen self-amplifying RNA SARS-CoV-2 vaccine induces potent humoral and cellular immune responses and protects against SARS-CoV-2 variants through T cell-

908 mediated immunity. Mol. Ther. 30, 2968-2983.
909 https://doi.org/10.1016/j.ymthe.2022.04.014.
910
911 McKay, P.F., Hu, K., Blakney, A.K., Samnuan, K., Brown, J.C., Penn, R., Zhou, J.,
912 Bouton, C.R., Rogers, P., Polra, K., et al. (2020). Self-amplifying RNA SARS-CoV-2 lipid
913 nanoparticle vaccine candidate induces high neutralizing antibody titers in mice. Nat.
914 Commun. 11, 3523. https://doi.org/10.1038/s41467-020-17409-9.
915
916 Mehdi, F., Chattopadhyay, S., Thiruvengadam, R., Yadav, S., Kumar, M., Sinha, S.K.,
917 Goswami, S., Kshetrapal, P., Wadhwa, N., Chandramouli Natchu, U., et al. (2021).
918 Development of a fast SARS-CoV-2 IgG ELISA, based on receptor-binding domain, and
919 its comparative evaluation using temporally segregated samples from RT-PCR positive
920 individuals. Front. Microbio. 11, 618097. https://doi.org/10.3389/fmicb.2020.618097.
921
922 Oda, Y., Kumagai, Y., Kanai, M., Iwama, Y., Okura, I., Minamida, T., Yagi, Y., Kurosawa,
923 T., Greener, B., Zhang, Y., et al. (2024) Immunogenicity and safety of a booster dose of
924 a self-amplifying RNA COVID-19 vaccine (ARCT-154) versus BNT162b2 mRNA COVID-
925 19 vaccine: a double-blind, multicentre, randomised, controlled, phase 3, non-inferiority
926 trial. Lancet Infect. Dis. 24, 351-360. https://doi.org/10.1016/S1473-3099(23)00650-3.
927
928 Parhiz, H., Atochina-Vasserman, E.N., Weissman, D. (2024). mRNA-based therapeutics:
929 looking beyond COVID-19 vaccines. The Lancet 403, 1192-1204.
930 https://doi.org/10.1016/S0140-6736(23)02444-3.
931
932 Piccoli, L., Park, Y.J., Tortorici, M.A., Czudnochowski, N., Walls, A.C., Beltramello, M.,
933 Silacci-Fregni, C., Pinto, D., Rosen, L.E., Bowen, J.E., et al. (2020). Mapping
934 Neutralizing and Immunodominant Sites on the SARS-CoV-2 Spike Receptor-Binding
935 Domain by Structure-Guided High-Resolution Serology. Cell 183, 1024-1042.
936 https://doi.org/10.1016/j.cell.2020.09.037.
937
938 Planas, D., Saunders, N., Maes, P., Guivel-Benhassine, F., Planchais, C., Buchrieser, J.,
939 Bolland, W.H., Porrot, F., Staropoli, I., Lemoine, F., et al. (2022).
940 https://doi.org/Considerable escape of SARS-CoV-2 Omicron to antibody neutralization.
941 Nature 602, 671-675. https://doi.org/10.1038/s41586-021-04389-z.
942
943 Pollock, K.M., Cheeseman, H.M., Szubert, A.J., Libri, V., Boffito, M., Owen, D., Bern, H.,
944 McFarlane, L.R., O'Hara, J., Lemm, N.M., et al. (2022). Safety and immunogenicity of a
945 self-amplifying RNA vaccine against COVID-19: COVAC1, a phase I, dose-ranging trial.
946 EClinicalMedicine 44, 101262. https://doi.org/10.1016/j.eclinm.2021.101262.
947
948 Qu, L., Yi, Z., Shen, Y., Lin, L., Chen, F., Xu, Y., Wu, Z., Tang, H., Zhang, X., Tian, F., et
949 al. (2022). Circular RNA vaccines against SARS-CoV-2 and emerging variants. Cell 185,
950 1728-1744 e1716. https://doi.org/10.1016/j.cell.2022.03.044.
951
952 Routhu, N.K., Cheedarla, N., Bollimpelli, V.S., Gangadhara, S., Edara, V.V., Lai, L.,
953 Sahoo, A., Shiferaw, A., Styles, T.M., Floyd, K., et al. (2021). SARS-CoV-2 RBD trimer
954 protein adjuvanted with Alum-3M-052 protects from SARS-CoV-2 infection and immune
955 pathology in the lung. Nat. Commun. 12, 3587. https://doi.org/10.1038/s41467-021-
956 23942-y.
957
958 Saraf, A., Gurjar, R., Kaviraj, S., Kulkarni, A., Kumar, D., Kulkarni, R., Virkar, R.,
959 Krishnan, J., Yadav, A., Baranwal, E., et al. (2024). An Omicron-specific, self-amplifying
960 mRNA booster vaccine for COVID-19: a phase 2/3 randomized trial. Nat. Med. 30, 1363-
961 1372. https://doi.org/10.1038/s41591-024-02955-2.
962
963 Schmidt, C., Schnierle, B.S. (2023). Self-Amplifying RNA Vaccine Candidates:
964 Alternative Platforms for mRNA Vaccine Development. Pathogens 12.
965 https://doi.org/10.3390/pathogens12010138.
966

Seephetdee, C., Bhukhai, K., Buasri, N., Leelukkanaveera, P., Lerdwattanasombat, P., Manopwisedjaroen, S., Phueakphud, N., Kuhaudomlarp, S., Olmedillas, E., Saphire, E.O., et al.(2022). A circular mRNA vaccine prototype producing VFLIP-X spike confers a broad neutralization of SARS-CoV-2 variants by mouse sera. Antiviral Res. 204, 105370. https://doi.org/10.1016/j.antiviral.2022.105370.

Tao, K., Tzou, P.L., Nouhin, J., Gupta, R.K., de Oliveira, T., Kosakovsky Pond, S.L., Fera, D., Shafer, R.W. (2021). The biological and clinical significance of emerging SARS-CoV-2 variants. Nat. Rev. Genet. 22, 757-773. https://doi.org/10.1038/s41576-021-00408-x

Thomas, S.J., Moreira Jr, E.D., Kitchin, N., Absalon, J., Gurtman, A., Lockhart, S., Perez, J.L., Pérez Marc, G., Polack, F.P., Zerbini, C., Bailey, R., et al. (2021). Safety and efficacy of the BNT162b2 mRNA Covid-19 vaccine through 6 months. N. Engl. J. Med. 385, 1761-1773. https://doi.org/10.1056/NEJMoa2110345.

Verma, R., Saha, S., Kumar, S., Mani, S., Maiti, T.K., Surjit, M. (2021). RNA-protein interaction analysis of SARS-CoV-2 5′ and 3′ untranslated regions reveals a role of lysosome-associated membrane protein-2a during viral infection. mSystems 6, 00643-00621. https://doi.org/10.1128/mSystems.00643-21.

Wang, X., Lu, Z., Gomez, A., Hon, G.C., Yue, Y., Han, D., Fu, Y., Parisien, M., Dai, Q., Jia, G., et al. (2014). N6-methyladenosine-dependent regulation of messenger RNA stability. Nature 505, 117-120. https://doi.org/10.1038/nature12730.

Weaver, S.C., Salas, R., Rico-Hesse, R., Ludwig, G.V., Oberste, M.S., Boshell, J., Tesh, R.B. (1996). Re-emergence of epidemic Venezuelan equine encephalomyelitis in South America. Lancet 348, 436-440. https://doi.org/10.1016/s0140-6736(96)02275-1.

Wesselhoeft, R.A., Kowalski, P.S., Anderson, D.G. (2018). Engineering circular RNA for potent and stable translation in eukaryotic cells. Nat. Commun. 9, 2629. https://doi.org/10.1038/s41467-018-05096-6.

Wesselhoeft, R.A., Kowalski, P.S., Parker-Hale, F.C., Huang, Y., Bisaria, N., Anderson, D.G. (2019). RNA circularization diminishes immunogenicity and can extend translation duration in vivo. Mol. cell 74, 508-520. e504. https://doi.org/10.1016/j.molcel.2019.02.015.

Yuan, Y., Zhang, X., Chen, R., Li, Y., Wu, B., Li, R., Zou, F., Ma, X., Wang, X., Chen, Q., et al. (2022). A bivalent nanoparticle vaccine exhibits potent cross-protection against the variants of SARS-CoV-2. Cell Rep. 38, 110256. https://doi.org/10.1016/j.celrep.2021.110256.

Zhou, J., Ye, T., Yang, Y., Li, E., Zhang, K., Wang, Y., Chen, S., Hu, J., Zhang, K., Liu, F., et al. (2024). Circular RNA vaccines against monkeypox virus provide potent protection against vaccinia virus infection in mice. Mol. Ther. 32, 1779–1789. https://doi.org/10.1016/j.ymthe.2024.04.028.

Figure 1

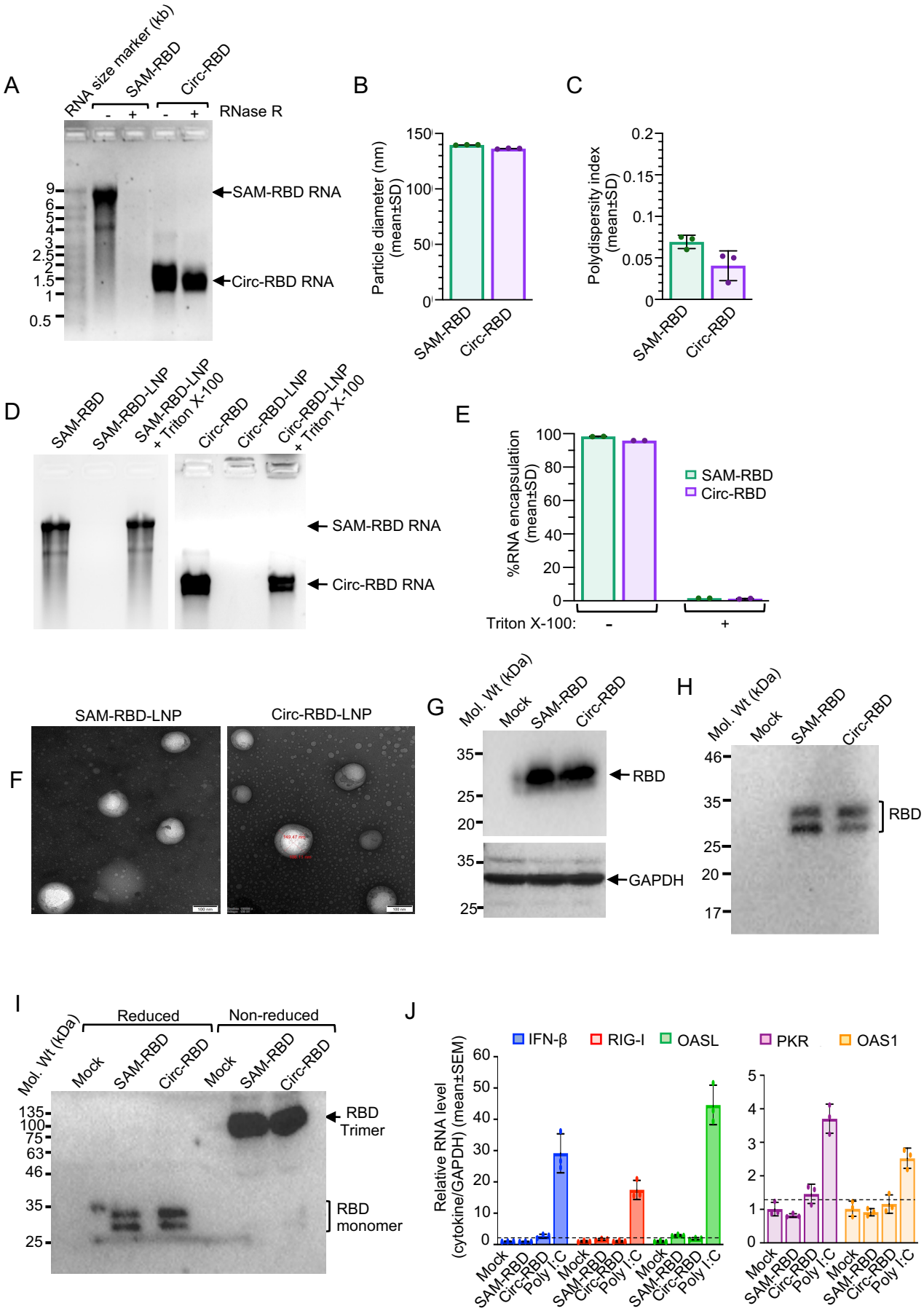
A
RNA size marker (kb)
SAM-RBD
Circ-RBD
RNase R
- + - +
9
6
5
4
3
2.5
2
1.5
1
0.5
SAM-RBD RNA
Circ-RBD RNA
B
Particle diameter (nm) (mean±SD)
150
100
50
0
SAM-RBD
Circ-RBD
C
Polydispersity index (mean±SD)
0.2
0.15
0.1
0.05
0
SAM-RBD
Circ-RBD
D
SAM-RBD
SAM-RBD-LNP
SAM-RBD-LNP + Triton X-100
Circ-RBD
Circ-RBD-LNP
Circ-RBD-LNP + Triton X-100
SAM-RBD RNA
Circ-RBD RNA
E
%RNA encapsulation (mean±SD)
100
80
60
40
20
0
SAM-RBD
Circ-RBD
Triton X-100: - +
F
SAM-RBD-LNP
Circ-RBD-LNP
G
Mol. Wt (kDa)
Mock
SAM-RBD
Circ-RBD
35
25
20
RBD
35
25
GAPDH
H
Mol. Wt (kDa)
Mock
SAM-RBD
Circ-RBD
46
35
25
20
17
RBD
I
Mol. Wt (kDa)
Reduced
Non-reduced
Mock
SAM-RBD
Circ-RBD
Mock
SAM-RBD
Circ-RBD
135
100
75
63
46
35
25
RBD Trimer
RBD monomer
J
IFN-β
RIG-I
OASL
PKR
OAS1
Relative RNA level (cytokine/GAPDH) (mean±SEM)
60
50
40
30
20
10
0
5
4
3
2
1
0
Mock
SAM-RBD
Circ-RBD
Poly I:C

1023 **Figure legends**

1024

1025 **Figure 1. Production and characterization of the self-amplifying and circular RNA**
1026 **vaccine candidates.**

1027 (A) Agarose gel electrophoresis analysis of *in vitro* transcribed and purified SAM-RBD and
1028 Circ-RBD RNA with (+) and without (-) treatment with RNase R .

1029 (B) Average particle size of SAM-RBD-RNA-LNP and Circ-RBD-RNA-LNP complex.

1030 (C) Average polydispersity Index of SAM-RBD-RNA-LNP and Circ-RBD-RNA-LNP complex.

1031 (D) Agarose gel electrophoresis analysis of SAM-RBD and Circ-RBD-RNA incorporation into
1032 the LNP on RNA-LNP formulation treated with Triton X-100, as indicated.

1033 (E) Average percent SAM-RBD and Circ-RBD RNA incorporation into the LNP on RNA-LNP
1034 formulation treated with Triton X-100, as indicated.

1035 (F) Scanning electron microscopy image of SAM-RBD-LNP and Circ-RBD LNP. Scale:100nm.

1036 (G) Western blot analysis of RBD protein in HEK239T cells transfected with SAM-RBD and
1037 Circ-RBD RNA (upper panel). Mock: Lysate from HEK293T cells treated with LNP. Lower
1038 panel: Anti GAPDH western blot of aliquots of cell lysate used in the upper panel.

1039 (H) Anti-RBD western blot of RBD protein in the cell culture medium of HEK239T cells
1040 mentioned in (G).

1041 (I) Anti-RBD western blot of aliquots of sample used in (H) under reducing and non-reducing
1042 conditions, as indicated.

1043 (J) RT-qPCR analysis of the indicated genes in total RNA isolated from HEK239T cells
1044 transfected with SAM-RBD or Circ-RBD-RNA, as indicated. Mock: lipofectamine 3000
1045 transfected cells. A set of samples from poly I:C transfected cells were simultaneously
1046 processed, as positive control. Dotted line indicates the background level. Data are mean±SD
1047 of three independent experiments. *P*-values were calculated by the non-parametric student's
1048 t-test, using the Mann-Whitney test.

1049

1050

1051

1052

1053

1054

1055

1056

1057

1058

1059

1060

Figure 2

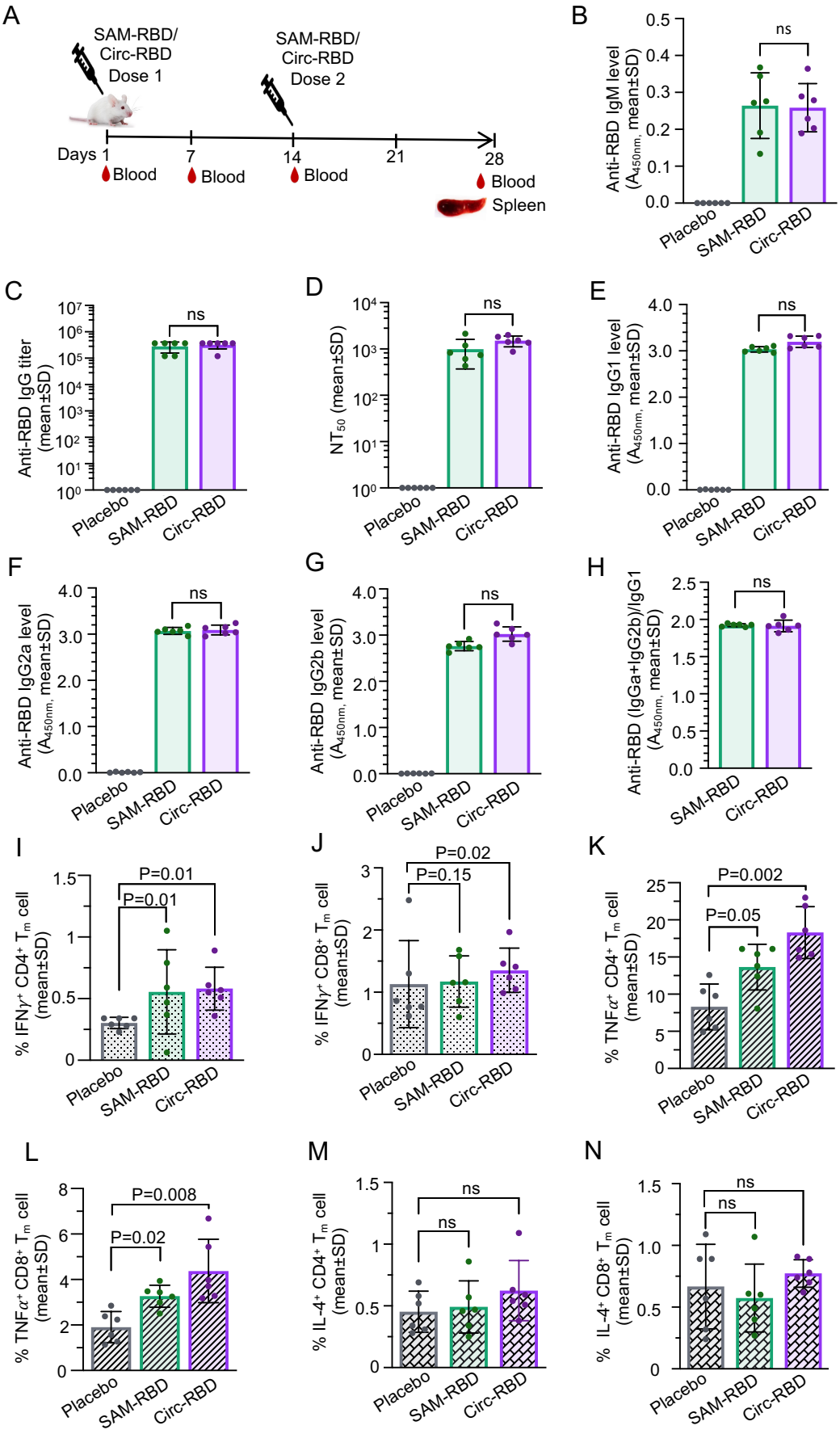
A
SAM-RBD/
Circ-RBD
Dose 1
SAM-RBD/
Circ-RBD
Dose 2
Days 1
7
14
21
28
Blood
Blood
Blood
Blood
Spleen
B
Anti-RBD IgM level
(A_{450nm}, mean±SD)
ns
C
Anti-RBD IgG titer
(mean±SD)
ns
D
NT_{50} (mean±SD)
ns
E
Anti-RBD IgG1 level
(A_{450nm}, mean±SD)
ns
F
Anti-RBD IgG2a level
(A_{450nm}, mean±SD)
ns
G
Anti-RBD IgG2b level
(A_{450nm}, mean±SD)
ns
H
Anti-RBD (IgGa+IgG2b)/IgG1
(A_{450nm}, mean±SD)
ns
I
% IFNγ+ CD4+ Tm cell
(mean±SD)
P=0.01
P=0.01
J
% IFNγ+ CD8+ Tm cell
(mean±SD)
P=0.02
P=0.15
K
% TNFα+ CD4+ Tm cell
(mean±SD)
P=0.002
P=0.05
L
% TNFα+ CD8+ Tm cell
(mean±SD)
P=0.008
P=0.02
M
% IL-4+ CD4+ Tm cell
(mean±SD)
ns
ns
N
% IL-4+ CD8+ Tm cell
(mean±SD)
ns
ns
Placebo
SAM-RBD
Circ-RBD

1061 **Figure 2. Immunogenicity assessment of SAM-RBD and Circ-RBD-RNA vaccine**
1062 **formulations.**
1063 (A) Schematic of the immunization study. Balb/c mice were intradermally injected with 10μg
1064 SAM-RBD or Circ-RBD-RNA-LNP on day 1 and 14. Blood was collected via retro-orbital route
1065 prior to the first immunization and subsequently on day 7 and day 28. Animals were euthanized
1066 on day 28, blood and spleen were collected.
1067 (B) Anti-RBD IgM level at 1 week post-immunization in the sera (1:500 dilution) of mice
1068 injected with the placebo (PBS), SAM-RBD and Circ-RBD-LNP, evaluated by ELISA.
1069 (C) Anti-RBD IgG titre at 4 weeks post-immunization in the sera of mice described in (B),
1070 evaluated by ELISA.
1071 (D) 50% virus neutralization titre (NT_{50}) at 4 weeks post-immunization in the sera of mice
1072 described in (B), evaluated by PRNT assay.
1073 (E) Anti-RBD IgG1 level (1:500 dilution) at 4 weeks post-immunization in the sera of mice
1074 described in (B), evaluated by ELISA.
1075 (F) Anti-RBD IgG2a level (1:500 dilution) at 4 weeks post-immunization in the sera of mice
1076 described in (B), evaluated by ELISA.
1077 (G) Anti-RBD IgG2b level (1:500 dilution) at 4 weeks post-immunization in the sera of mice
1078 described in (B), evaluated by ELISA.
1079 (H) Ratio of anti-RBD T_H1 antibody (IgG2a and IgG2b) to T_H2 (IgG1) antibody in the sera of
1080 mice injected with the SAM-RBD and Circ-RBD at 4 weeks, evaluated by ELISA.
1081 (I) Percentage of IFNγ and CD4 positive T-cells in the splenocytes, following stimulation with
1082 the SARS-CoV-2-Spike-RBD peptide pool, evaluated by FACS.
1083 (J) Percentage of IFNγ and CD8 positive T-cells in the splenocytes, following stimulation with
1084 the SARS-CoV-2-Spike-RBD peptide pool, evaluated by FACS.
1085 (K) Percentage of TNFα and CD4 positive T-cells in the splenocytes, following stimulation with
1086 the SARS-CoV-2-Spike-RBD peptide pool, evaluated by FACS.
1087 (L) Percentage of TNFα and CD8 positive T-cells in the splenocytes, following stimulation with
1088 the SARS-CoV-2-Spike-RBD peptide pool, evaluated by FACS.
1089 (M) Percentage of IL-4 and CD4 positive T-cells in the splenocytes, following stimulation with
1090 the SARS-CoV-2-Spike-RBD peptide pool, evaluated by FACS.
1091 (N) Percentage of IL-4 and CD8 positive T-cells in the splenocytes, following stimulation with
1092 the SARS-CoV-2- Spike-RBD peptide pool, evaluated by FACS.
1093 In all images, bars represent the average and dots represent the value obtained from each
1094 animal. Data are mean±SD, *p*-values were calculated by the non-parametric student's t-test,
1095 using the Mann-Whitney test (B-H) and the non-parametric one-way ANOVA, using the
1096 Kruskal-wallis test (I-N). Values showing distinct difference from the majority in the group were
1097 not considered for calculating the *p*-value in the panels I-L.
1098
1099

Figure 3

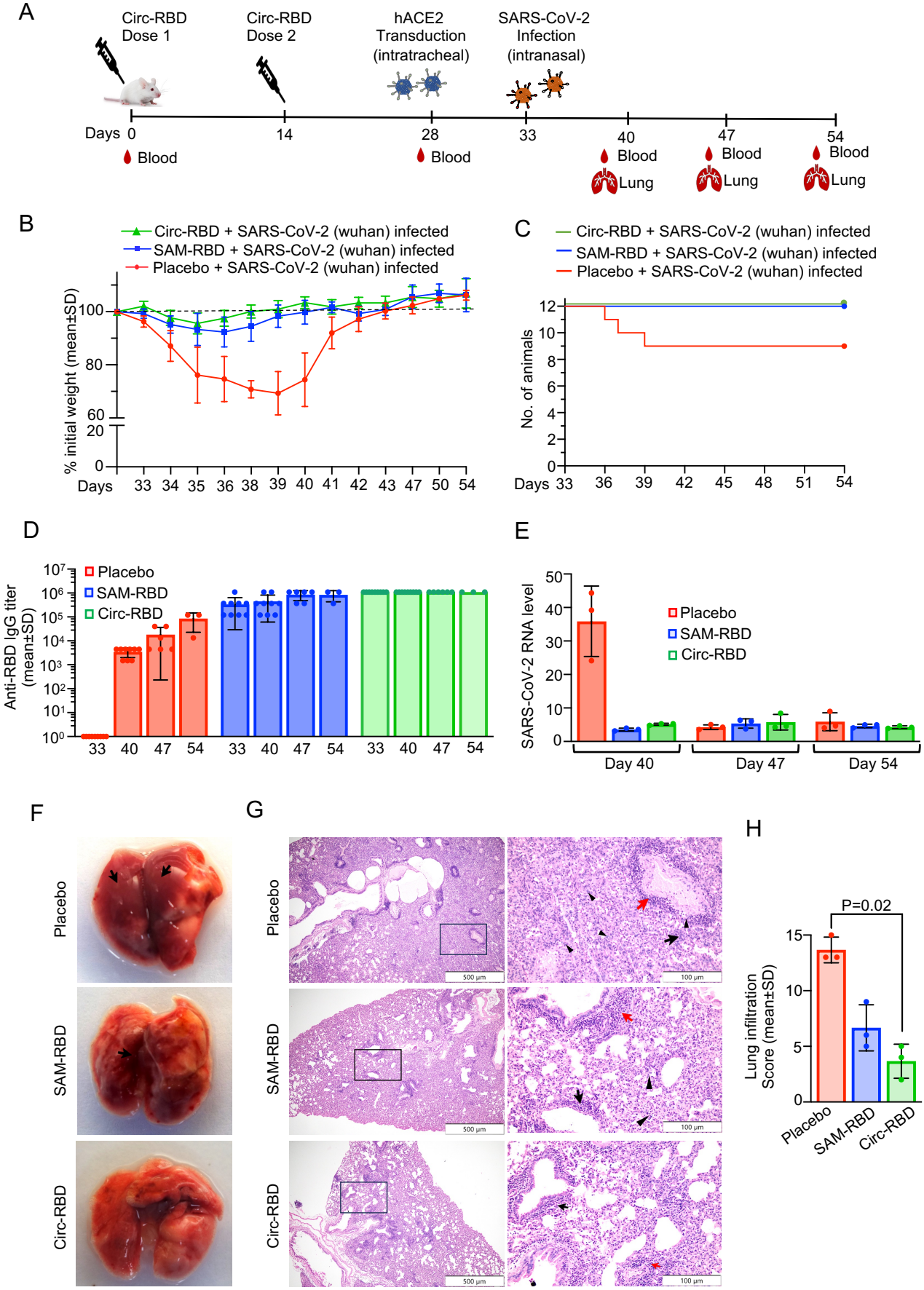
A
Circ-RBD Dose 1
Circ-RBD Dose 2
hACE2 Transduction (intratracheal)
SARS-CoV-2 Infection (intranasal)
Days 0 14 28 33 40 47 54
Blood
Lung
B
Circ-RBD + SARS-CoV-2 (wuhan) infected
SAM-RBD + SARS-CoV-2 (wuhan) infected
Placebo + SARS-CoV-2 (wuhan) infected
% initial weight (mean±SD)
Days 33 34 35 36 38 39 40 41 42 43 47 50 54
C
No. of animals
Days 33 36 39 42 45 48 51 54
D
Anti-RBD IgG titer (mean±SD)
Placebo
SAM-RBD
Circ-RBD
E
SARS-CoV-2 RNA level
Day 40
Day 47
Day 54
F
G
H
P=0.02
Lung infiltration Score (mean±SD)
Placebo
SAM-RBD
Circ-RBD

1100 **Figure 3. Immunization with SAM-RBD and Circ-RBD RNA vaccines protect mice from**
1101 **intratracheal SARS-CoV-2 challenge-induced disease symptoms.**
1102 (A) Schematic of immunization and challenge study. Blood was collected before immunization
1103 on day 0 and day 14. Intratracheal transduction of hACE2-adenovirus was done on day 28,
1104 followed by intranasal infection with SAR-CoV-2 (Wuhan) on day 33. Mouse weight was
1105 measured every day from day 33-54. Mice were sacrificed (3 animals at each time point) on
1106 day 40, 47 and 54 and blood and lung tissues were collected.
1107 (B) Weight of each mouse in placebo, SAM-RBD and Circ-RBD RNA vaccine immunization
1108 group was measured every day from day 33-54 and the percent weight change with respect
1109 to the weight on day 33 (considered 100%) is plotted in the graph.
1110 (C) Survival of mice in placebo, SAM-RBD and Circ-RBD RNA vaccine immunized groups
1111 were monitored every day from day 33-54.
1112 (D) Anti-RBD IgG titer in the sera of placebo, SAM-RBD and Circ-RBD RNA vaccine
1113 immunized, SARS-CoV-2 (Wuhan) infected mice as indicated in (A). Sera collected on day
1114 40, 47 and 54 were evaluated by ELISA.
1115 (E) Measurement of viral RNA level in aliquots of the lung tissue of placebo, SAM-RBD and
1116 Circ-RBD RNA vaccine immunized, SARS-CoV-2 (Wuhan) infected mice as indicated in (A).
1117 Viral RNA level was determined by RT-qPCR in samples collected on day 40, 47 and 54.
1118 (F) Lung morphology of the placebo, SAM-RBD and Circ-RBD RNA vaccine immunized,
1119 SARS-CoV-2 (Wuhan) infected mice, collected on day 40.
1120 (G) Representative H&E stained image of lung tissue section prepared from placebo, SAM-
1121 RBD or Circ-RBD RNA vaccine immunized, SARS-CoV-2 (Wuhan) infected mice, collected
1122 on day 40. Image were acquired at 40X (left panel) and 200X magnification (right panel). Black
1123 and red arrows indicate peribronchiolar and perialveolar infiltration, respectively. Black arrow-
1124 head indicates neutrophil infiltration.
1125 (H) Lung infiltration score of placebo, SAM-RBD and Circ-RBD RNA vaccine immunized,
1126 SARS-CoV-2 (Wuhan) infected mice, evaluated by analysis of H&E stained images of tissue
1127 sections prepared from lungs collected on day 40.
1128 In (B), (D), (E) and (H) , data are shown as the mean±SD and significance was determined
1129 using unpaired student's t-test, Mann-Whitney test.
1130
1131
1132
1133
1134
1135
1136
1137

Figure 4

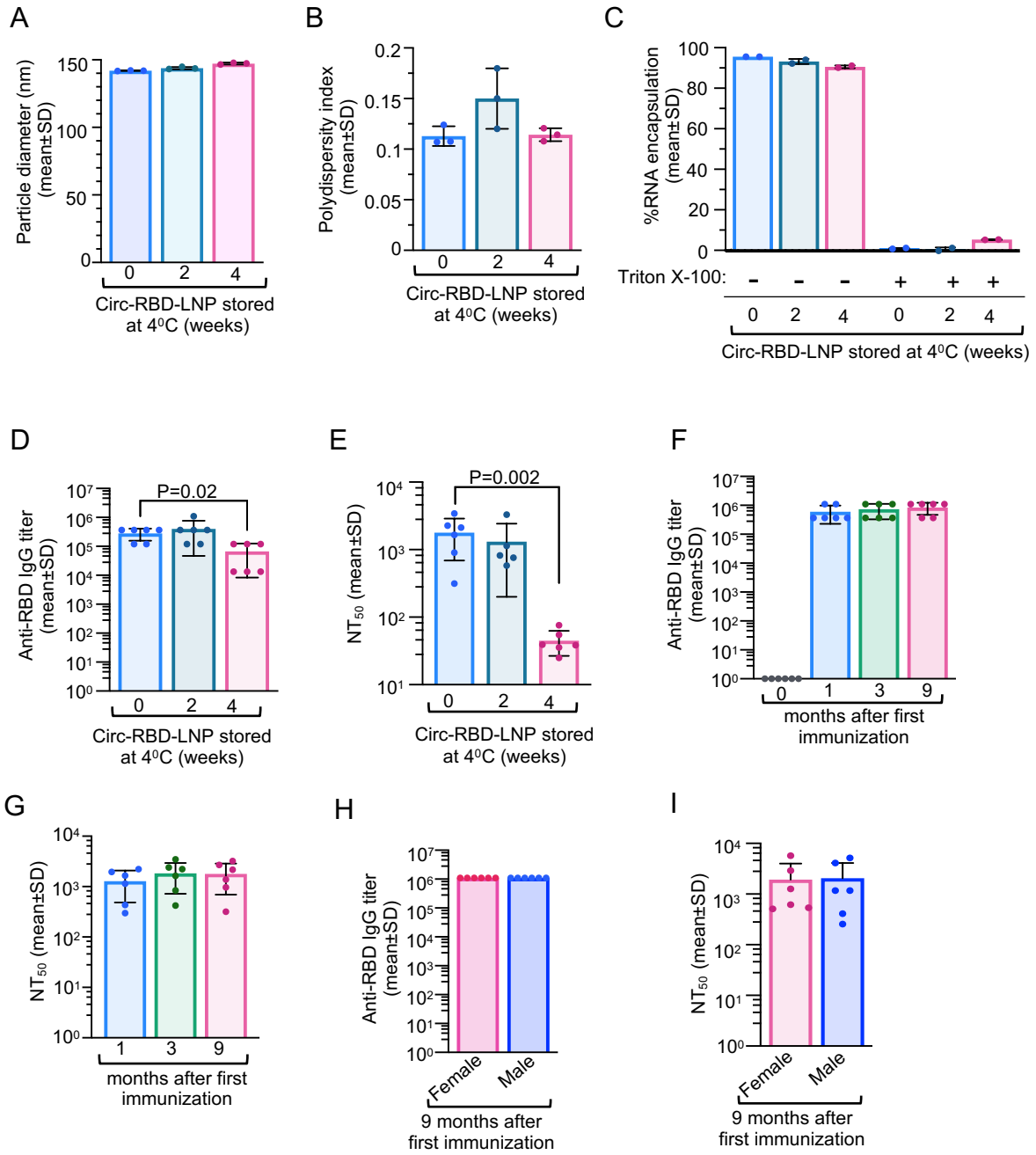
A
Particle diameter (nm) (mean±SD)
150
100
50
0
0
2
4
Circ-RBD-LNP stored at 4⁰C (weeks)
B
Polydispersity index (mean±SD)
0.2
0.15
0.1
0.05
0
0
2
4
Circ-RBD-LNP stored at 4⁰C (weeks)
C
%RNA encapsulation (mean±SD)
100
80
60
40
20
0
Triton X-100: - - - + + +
0 2 4 0 2 4
Circ-RBD-LNP stored at 4⁰C (weeks)
D
Anti-RBD IgG titer (mean±SD)
P=0.02
0 2 4
Circ-RBD-LNP stored at 4⁰C (weeks)
E
NT50 (mean±SD)
P=0.002
0 2 4
Circ-RBD-LNP stored at 4⁰C (weeks)
F
Anti-RBD IgG titer (mean±SD)
0 1 3 9
months after first immunization
G
NT50 (mean±SD)
1 3 9
months after first immunization
H
Anti-RBD IgG titer (mean±SD)
Female
Male
9 months after first immunization
I
NT50 (mean±SD)
Female
Male
9 months after first immunization

1138 **Figure 4. Stability and durability of the immune response induced by the Circ-RBD-LNP**
1139 **vaccine formulation.**
1140 (A) Average size of the Circ-RBD-LNP stored at 4^0C for 0, 2 and 4 weeks, evaluated by
1141 dynamic light scattering.
1142 (B) Average polydispersity index of the Circ-RBD-LNP, stored as indicated in (A).
1143 (C) Percentage of RNA encapsulated into the LNP in the Circ-RBD-LNP formulation, stored
1144 as indicated in (A). Equal aliquots of the samples were treated with the Triton X-100.
1145 (D) Anti-RBD IgG titre in the sera of mice immunized for 4 weeks with the Circ-RBD-LNP,
1146 stored as indicated in (A).
1147 (E) 50% virus neutralization titre (NT_{50}) in aliquots of the sera used in (D), evaluated by PRNT
1148 assay.
1149 (F) Anti-RBD IgG titre at 0, 1, 3 and 9 months post-immunization in the sera of mice immunized
1150 with the Circ-RBD-LNP, evaluated by ELISA.
1151 (G) 50% virus neutralization titre (NT_{50}) in aliquots of the sera described in (F), evaluated by
1152 PRNT assay.
1153 (H) Anti-RBD IgG titre at 9 months post-immunization with the Circ-RBD-LNP, in male and
1154 female mice, evaluated by ELISA.
1155 (I) 50% virus neutralization titre (NT_{50}) in aliquots of the sera described in (H), evaluated by
1156 PRNT assay.
1157 Data are mean±SD of triplicate samples (A-C) and six mice/group (D-I), *p*-values were
1158 determined by the unpaired student's t-test, using the Mann-Whitney test.
1159
1160
1161
1162
1163
1164
1165
1166
1167
1168
1169
1170
1171
1172
1173
1174
1175

Figure 5

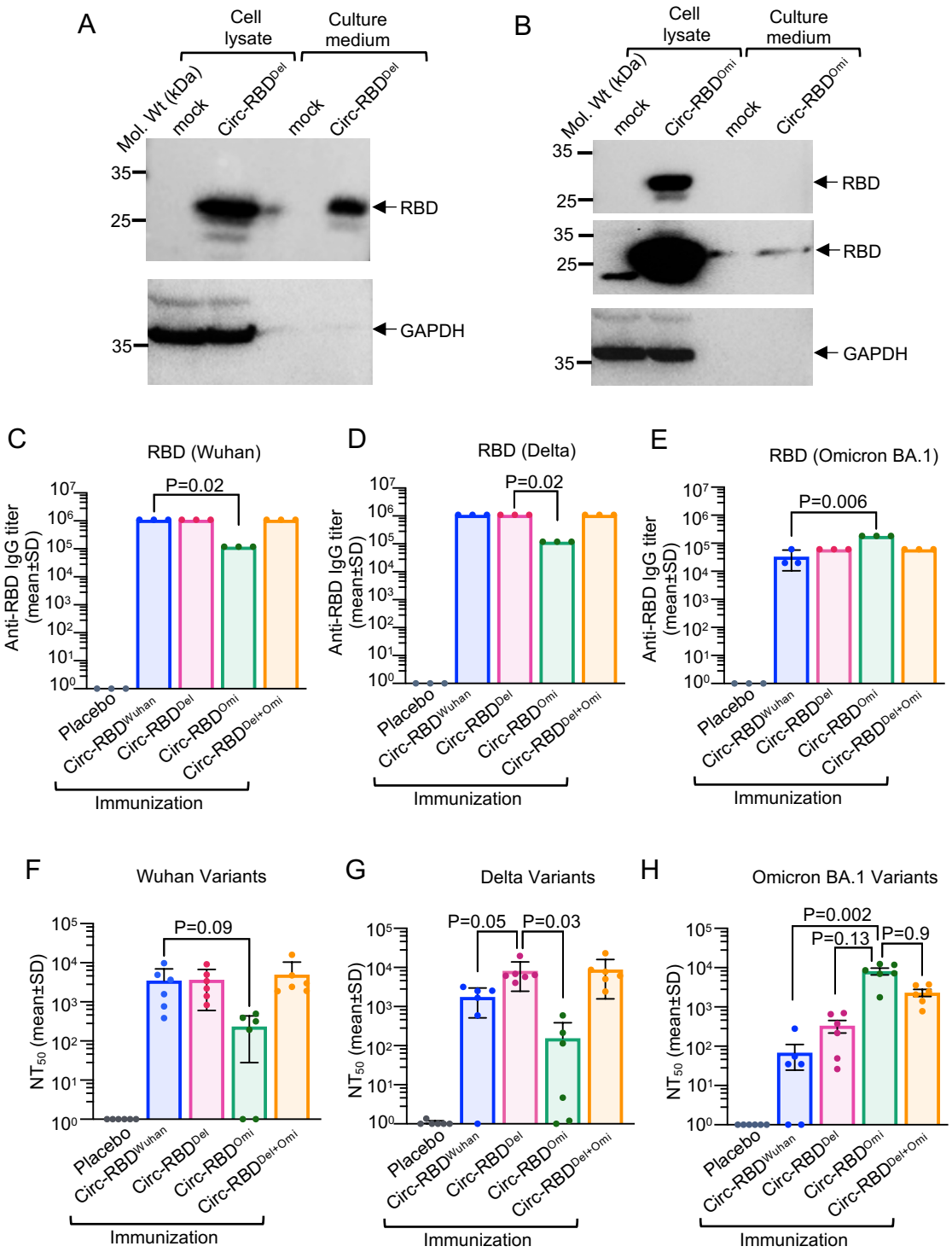
A
Cell lysate
Culture medium
Mol. Wt (kDa)
mock
Circ-RBD^{Del}
mock
Circ-RBD^{Del}
35
25
RBD
35
GAPDH
B
Cell lysate
Culture medium
Mol. Wt (kDa)
mock
Circ-RBD^{Omi}
mock
Circ-RBD^{Omi}
35
25
RBD
35
25
RBD
35
GAPDH
C
RBD (Wuhan)
P=0.02
Anti-RBD IgG titer (mean±SD)
Placebo
Circ-RBD^{Wuhan}
Circ-RBD^{Del}
Circ-RBD^{Omi}
Circ-RBD$^{Del+Omi}$
Immunization
D
RBD (Delta)
P=0.02
Anti-RBD IgG titer (mean±SD)
Placebo
Circ-RBD^{Wuhan}
Circ-RBD^{Del}
Circ-RBD^{Omi}
Circ-RBD$^{Del+Omi}$
Immunization
E
RBD (Omicron BA.1)
P=0.006
Anti-RBD IgG titer (mean±SD)
Placebo
Circ-RBD^{Wuhan}
Circ-RBD^{Del}
Circ-RBD^{Omi}
Circ-RBD$^{Del+Omi}$
Immunization
F
Wuhan Variants
P=0.09
NT_{50} (mean±SD)
Placebo
Circ-RBD^{Wuhan}
Circ-RBD^{Del}
Circ-RBD^{Omi}
Circ-RBD$^{Del+Omi}$
Immunization
G
Delta Variants
P=0.05
P=0.03
NT_{50} (mean±SD)
Placebo
Circ-RBD^{Wuhan}
Circ-RBD^{Del}
Circ-RBD^{Omi}
Circ-RBD$^{Del+Omi}$
Immunization
H
Omicron BA.1 Variants
P=0.002
P=0.13
P=0.9
NT_{50} (mean±SD)
Placebo
Circ-RBD^{Wuhan}
Circ-RBD^{Del}
Circ-RBD^{Omi}
Circ-RBD$^{Del+Omi}$
Immunization

1176 **Figure 5. Assessment of immunogenicity and virus neutralization potential of the Circ-**
1177 **RBD^{Del} and Circ-RBD^{Omi} bivalent vaccine formulation.**
1178 (A) Western blot analysis of the RBD protein in the HEK239T cells transfected with the Circ-
1179 RBD-Delta RNA (upper panel). Mock: HEK293T cells treated with LNP. Lower panel: Anti
1180 GAPDH western blot of aliquots of the samples used in the upper panel.
1181 (B) Western blot analysis of the RBD protein in the HEK239T cells transfected with the Circ-
1182 RBD-Omicron-BA.1 RNA (upper panel-lower exposure, middle panel-higher exposure of the
1183 same blot). Mock: HEK293T cells treated with LNP. Lower panel: anti GAPDH western blot of
1184 aliquots of the samples used in the upper panel.
1185 (C) Anti-RBD-wuhan IgG titre at 4 weeks post-immunization in the sera of mice injected with
1186 the placebo (PBS), Circ-RBD^{Wuhan} , Circ-RBD^{Del}, Circ-RBD^{omi} and bivalent Circ-RBD$^{Del+omi}$
1187 vaccine formulations, evaluated by ELISA.
1188 (D) Anti-RBD-Delta IgG titre at 4 weeks post-immunization in the sera of mice described in
1189 (C), evaluated by ELISA.
1190 (E) Anti-RBD-Omicron IgG titre at 4 weeks post-immunization in the sera of mice described in
1191 (C), evaluated by ELISA.
1192 (F) 50% virus neutralization titre (NT_{50}) against the SARS-CoV-2 (Wuhan) at 4 weeks post-
1193 immunization in the sera of mice described in (C), evaluated by FRNT assay.
1194 (G) 50% virus neutralization titre (NT_{50}) against the SARS-CoV-2 (Delta) at 4 weeks post-
1195 immunization in the sera of mice described in (C), evaluated by FRNT assay.
1196 (H) 50% virus neutralization titre (NT_{50}) against the SARS-CoV-2 (Omicron BA.1) at 4 weeks
1197 post-immunization in the sera of mice described in (C), evaluated by FRNT assay.
1198 In (C)-(E), data are shown as the mean±SD from pooled sera of six mice, assayed in triplicate;
1199 in (F)-(H), data are shown as the mean±SD. *p*-values were determined by the non-parametric
1200 one-way ANOVA, using the Kruskal-wallis test.
1201
1202
1203
1204
1205
1206
1207
1208
1209
1210
1211
1212
1213

Figure S1

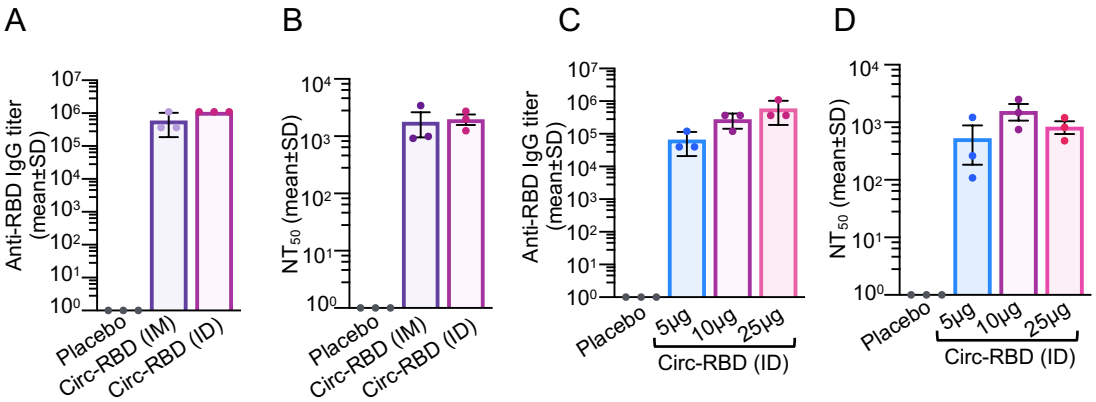
A
B
C
D
Anti-RBD IgG titer (mean±SD)
NT50 (mean±SD)
Placebo
Circ-RBD (IM)
Circ-RBD (ID)
5μg
10μg
25μg
Circ-RBD (ID)

1214 **Supplementary figure legends**

1215 **Figure S1. Selection of immunization route and dose of RNA-LNP formulation that**
1216 **elicits significant immune response in mice.**

1217 (A) Anti-RBD IgG titre at 4 weeks post-immunization in the sera of mice injected with the
1218 placebo (PBS) and the Circ-RBD-LNP via intramuscular (IM) or intradermal (ID) route,
1219 evaluated by ELISA.

1220 (B) 50% virus neutralization titre (NT_{50}) at 4 weeks post-immunization in the sera of mice
1221 described in (B), evaluated by PRNT assay.

1222 (C) Anti-RBD IgG titre at 4 weeks post-immunization in the sera of mice intradermally injected
1223 with the placebo (PBS) or 5, 10, 25μg of Circ-RBD-LNP, evaluated by ELISA.

1224 (D) 50% virus neutralization titre (NT_{50}) at 4 weeks post-immunization in the sera of mice
1225 described in (C), evaluated by PRNT assay.

1226 Data are shown as the mean±SD of pooled sera from five animals, assayed in triplicate; *p*-
1227 values were determined by the unpaired student's t-test, using the Mann-Whitney test.

1228
1229
1230
1231
1232
1233
1234
1235
1236
1237
1238
1239
1240
1241
1242
1243
1244
1245
1246
1247
1248
1249
1250

Figure S2

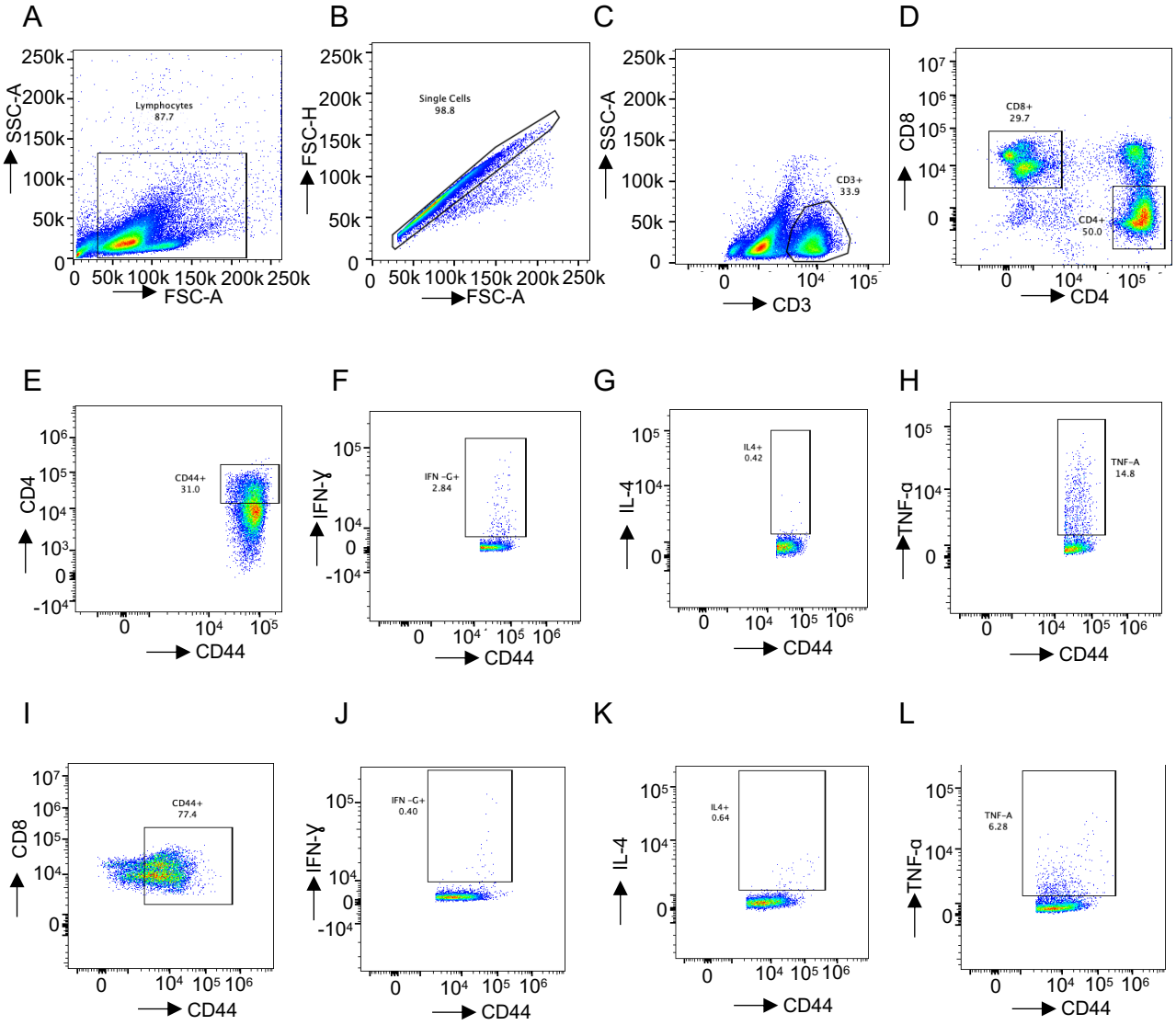
A
SSC-A
FSC-A
Lymphocytes
87.7
B
FSC-H
FSC-A
Single Cells
98.8
C
SSC-A
CD3
CD3+
33.9
D
CD8
CD4
CD8+
29.7
CD4+
50.0
E
CD4
CD44
CD44+
31.0
F
IFN-γ
CD44
IFN-G+
2.84
G
IL-4
CD44
IL4+
0.42
H
TNF-α
CD44
TNF-A
14.8
I
CD8
CD44
CD44+
77.4
J
IFN-γ
CD44
IFN-G+
0.40
K
IL-4
CD44
IL4+
0.64
L
TNF-α
CD44
TNF-A
6.28

1251 **Figure S2. Analysis of intracellular IFNγ, TNFα and IL-4 levels in the RBD peptide pool-**
1252 **stimulated CD4, CD8 positive T-cells derived from the splenocytes of Circ-RBD**
1253 **immunized mice.**
1254 (A)-(D) Representative FACS plot showing the gating strategy of lymphocytes (A), single cells
1255 (B), $CD3^+$ (C) and $CD4^+CD8^+$(D) T-cells.
1256 (E)-(H) Representative FACS plot showing the gating strategy of $CD4^+$ memory T-cells (E) and
1257 quantification of IFNγ (F), IL-4 (G) and TNFα (H) in $CD4^+$ memory T-cells.
1258 (I)-(L) Representative FACS plot showing the gating strategy of $CD8^+$ memory T-cell (J) and
1259 quantification of IFNγ (K), IL-4 (K) and TNFα (L) in $CD8^+$ memory T-cells.
1260
1261
1262
1263
1264
1265
1266
1267
1268
1269
1270
1271
1272
1273
1274
1275
1276
1277
1278
1279
1280
1281
1282
1283
1284
1285
1286
1287
1288

Figure S3

A

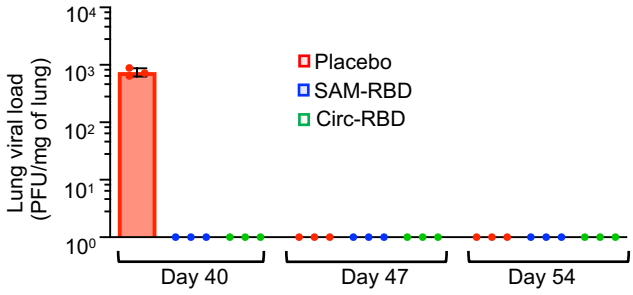

B

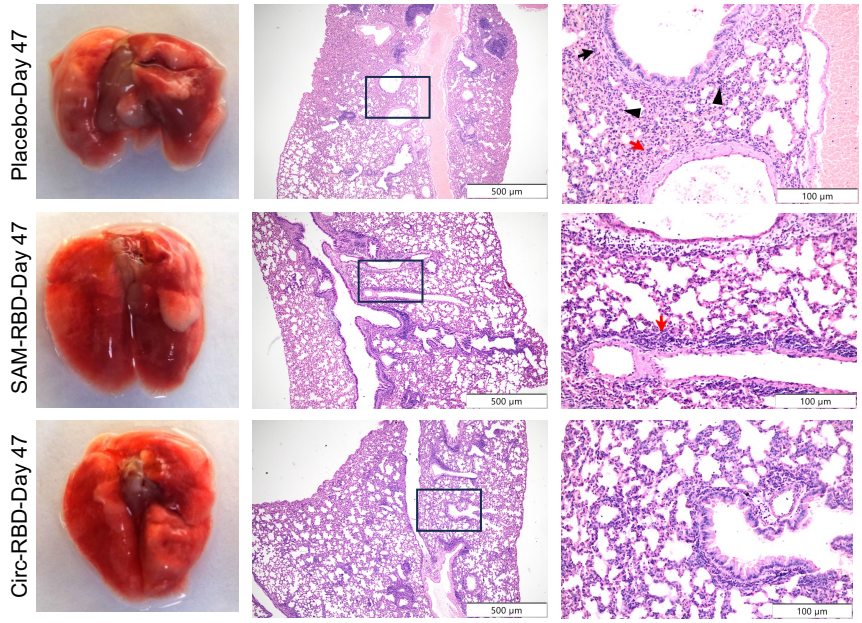

C

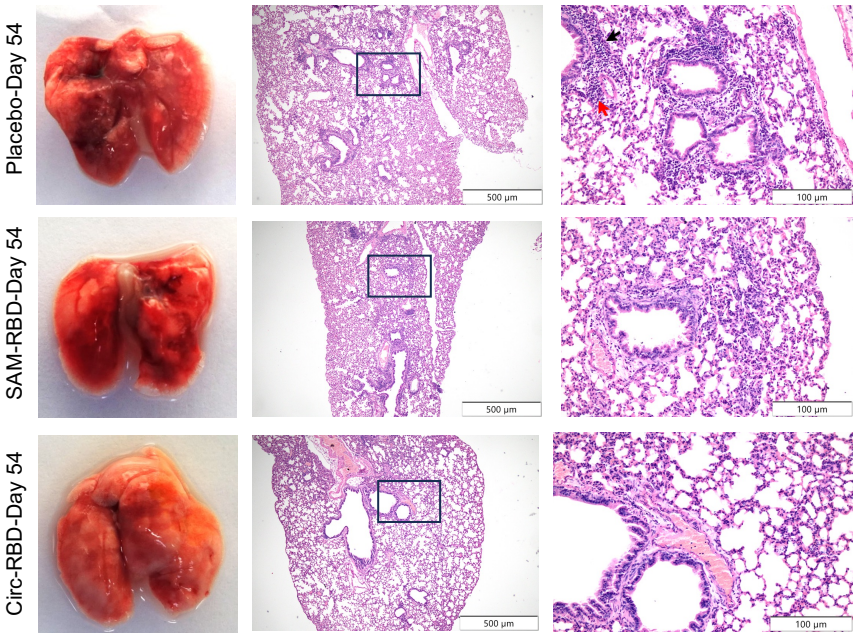

1289 **Figure S3. Immunization with the SAM-RBD and Circ-RBD RNA vaccines protect mice**
1290 **from intratracheal SARS-CoV-2 challenge.**
1291 (A) Measurement of viral load in aliquots of the lung tissue of placebo, SAM-RBD and Circ-
1292 RBD RNA vaccine immunized, SARS-CoV-2 (Wuhan) infected mice as indicated in Fig. 3A.
1293 Viral load was determined by plaque assay and represented as PFU/mg of lung in samples
1294 collected on day 40, 47 and 54.
1295 (B) Lung morphology of the placebo, SAM-RBD and Circ-RBD RNA vaccine immunized,
1296 SARS-CoV-2 (Wuhan) infected mice, collected on day 47 (left panel). Middle and right panels
1297 show representative H&E stained image of lung tissue section from samples shown in left
1298 panel. Images were acquired at 40X (middle panel) and 200X magnification (right panel).
1299 Black and red arrows indicate peribronchiolar and perialveolar infiltration, respectively, and
1300 black arrow-head indicates neutrophils.
1301 (C) Lung morphology of the placebo, SAM-RBD and Circ-RBD RNA vaccine immunized,
1302 SARS-CoV-2 (Wuhan) infected mice, collected on day 54 (left panel). Middle and right panels
1303 show representative H&E stained image of lung tissue section from samples shown in left
1304 panel. Images were acquired at 40X (middle panel) and 200X magnification (right panel).
1305 Black and red arrows indicate peribronchiolar and perialveolar infiltration, respectively.
1306
1307
1308
1309
1310
1311
1312
1313
1314
1315